

Minimum Distance Summaries for Robust Neural Posterior Estimation

Sherman Khoo¹ Dennis Prangle¹ Song Liu¹ Mark Beaumont²

Abstract

Simulation-based inference (SBI) enables amortized Bayesian inference by first training a neural posterior estimator (NPE) on prior-simulator pairs, typically through low-dimensional summary statistics, which can then be cheaply reused for fast inference by querying it on new test observations. Because NPE is estimated under the training data distribution, it is susceptible to misspecification when observations deviate from the training distribution. Many robust SBI approaches address this by modifying NPE training or introducing error models, coupling robustness to the inference network and compromising amortization and modularity. We introduce minimum-distance summaries, a plug-in robust NPE method that adapts queried test-time summaries independently of the pretrained NPE. Leveraging the maximum mean discrepancy (MMD) as a distance between observed data and a summary-conditional predictive distribution, the adapted summary inherits strong robustness properties from the MMD. We demonstrate that the algorithm can be implemented efficiently with random Fourier feature approximations, yielding a lightweight, model-free test-time adaptation procedure. We provide theoretical guarantees for the robustness of our algorithm and empirically evaluate it on a range of synthetic and real-world tasks, demonstrating substantial robustness gains with minimal additional overhead.

1. Introduction

Across many areas of science and engineering, including cosmology (Alsing et al., 2019), biology (Beaumont et al., 2002), and neuroscience (Lueckmann et al., 2017), stochastic simulators are widely used as mechanistic statistical models. Such simulators are able to encode rich domain

¹Department of Mathematics, University of Bristol, Bristol, UK

²Department of Biology, University of Bristol, Bristol, UK. Correspondence to: Sherman Khoo <sherman.khoo@bristol.ac.uk>.

Preprint. February 11, 2026.

knowledge, and are able to generate synthetic data for any candidate parameter, but their complexity makes statistical inference particularly challenging, as while simulating from the model is straightforward, the induced likelihood function $p(\mathbf{x} | \theta)$ is typically intractable or prohibitively expensive to evaluate, making standard likelihood-based inference challenging (Marin et al., 2012). This problem setting is known as likelihood-free inference, or simulation-based inference (SBI) (Cranmer et al., 2020).

Modern SBI methods are built around an *amortized* neural Bayesian inference paradigm, which is centered on training a conditional neural density estimator using simulated pairs (θ_i, \mathbf{x}_i) generated from the simulator model $p(\mathbf{x} | \theta)$ and the prior distribution $\pi(\theta)$ (Cranmer et al., 2020; Deistler et al., 2025). While these estimators can target the likelihood (Papamakarios et al., 2019), or density ratio (Cranmer et al., 2015; Hermans et al., 2020), we focus here on the canonical neural posterior estimator (NPE) (Papamakarios & Murray, 2016), which directly learns a mapping from observations (typically through a summary statistic \mathbf{s}) to the posterior $\mathbf{x} \rightarrow p(\theta | \mathbf{x})$. After an initial, computationally heavy, offline training stage for the density estimator, the resulting estimator enables fast test-time statistical inference with a cheap forward pass, thus amortizing computational costs across future downstream queries. This paradigm is particularly attractive for many scientific workflows where inference is repeated across many downstream datasets and experimental conditions. However, because amortized estimators are trained under the simulator’s prior predictive distribution $m(\mathbf{x}) = \int p(\mathbf{x} | \theta) \pi(\theta) d\theta$, they are brittle under model misspecification, where even a modest deviation from the true data-generating process (DGP) may lead to biased or unreliable posteriors (Ward et al., 2022; Schmitt et al., 2024). Hence, there has been a growing literature of robust SBI approaches aimed at addressing model misspecification (Kelly et al., 2025).

Model misspecification in SBI occurs when the true DGP lies outside of the simulator family (Cannon et al., 2022), operationally, this is reflected in the mismatch between the prior-predictive distribution and the DGP (Schmitt et al., 2024; Elsemüller et al., 2025), and minimizing this discrepancy has been a motivating principle for robust SBI approaches (Huang et al., 2023; Elsemüller et al., 2025). Although advances in robust SBI approaches have undoubt-

edly strengthened the real-world applicability of SBI, they often inherently couple robustness to the amortized inference engine, for instance, by requiring observations during NPE training (Huang et al., 2023), modifying the training objective of the amortized estimator (Gao et al., 2023), or augmenting the simulator with additional modeling components (Ward et al., 2022). This coupling reduces modularity and undermines the central benefit of amortization: reusing a single pretrained NPE for cheap, repeated inference across downstream queries.

In this work, we address model misspecification by reducing the gap between the simulator-induced distribution and true DGP, while adhering to the design principle of ensuring robustness without compromising amortization. Concretely, we keep the pretrained NPE $q_\psi(\theta | \mathbf{s})$ fixed and place adaptation entirely on the query side. At test time, we modify only the query, i.e., the observed data summary statistic \mathbf{s} , by adapting it such that it minimizes a robust discrepancy between an estimated summary-conditional data distribution and the empirical distribution of observations. We call the resulting adapted summary statistic a *minimum-distance summary*, and perform robust inference by querying the fixed amortized NPE with this adapted summary. Crucially, our procedure preserves the modularity and amortization property of SBI by separating robustness from inference, enabling post-hoc robustification of pretrained NPEs and flexible integration into realistic Bayesian data analysis workflows (Gelman et al., 2020). This separation aligns with the emerging trend towards reusable, general-purpose amortized SBI inference engines (Vetter et al., 2025; Gloeckler et al., 2024), where amortized models are intended to be reused across a broad set of tasks, making post-hoc, test-time robustification particularly desirable.

Our robust SBI approach aligns the data distribution and observations with a robust divergence, which we select as the maximum mean discrepancy (MMD) with a bounded characteristic kernel (Gretton et al., 2012), providing a robust, model-free objective for addressing misspecification. In order to provide a fast and lightweight estimation of the summary-conditional data distribution, we use a random Fourier feature approximation (Rahimi & Recht, 2007) which reduces the estimation to a regression problem, and yields a lightweight plug-in robustification that is fully decoupled from the amortized inference engine. Additionally, since misspecification is rarely known a priori, we use the same MMD objective as a misspecification sensitive diagnostic, only invoking test-time adaptation when misspecification is detected.

2. Background

Notation Let $\theta \in \Theta \subseteq \mathbb{R}^{d_\theta}$ denote the model parameters, with a prior density $\pi(\theta)$. We denote a single ob-

servation as $\mathbf{x} \in \mathcal{X} \subseteq \mathbb{R}^{d_x}$, and a dataset of N independent and identically distributed (i.i.d.) observations as $\mathbf{x}_{1:N} = \{\mathbf{x}_n\}_{n=1}^N \in \mathcal{X}^N$. Let $\mathcal{P}(\cdot)$ represent the space of Borel measures on a given sample space. The simulator model $\mathbb{P}_\theta \in \mathcal{P}(\mathcal{X})$ defines an implicit likelihood $p_\theta(\mathbf{x})$ for a single observation, and for a dataset of N i.i.d. observations we have the joint distribution $p_\theta(\mathbf{x}_{1:N}) = \prod_{n=1}^N p_\theta(\mathbf{x}_n)$. We denote observed datasets at test-time as $\tilde{\mathbf{x}}_{1:N}$ and the corresponding data-generating distribution as $\hat{\mathbb{P}}$. For convenience, we provide a table of key expressions in our manuscript, which will be defined in subsequent sections.

Symbol	Definition
$\mathbb{P}_{\mathbf{x} \mathbf{s}}$	Summary-conditional data distribution
$\hat{\mathbb{P}}_N$	Empirical distribution of observed dataset $\tilde{\mathbf{x}}_{1:N}$
$q_\psi(\theta \mathbf{s})$	Neural posterior estimator
$q_\omega(\mathbf{x} \mathbf{s})$	Decoder model
$f(\mathbf{x}_{1:N})$	Summary statistic function

2.1. Simulation-based inference

Simulation-based inference tackles Bayesian inference for implicit models \mathbb{P}_θ where the likelihood $p_\theta(\mathbf{x})$ is not tractable but simulations $\mathbf{x} \sim \mathbb{P}_\theta$ can be drawn for any choice of $\theta \in \Theta$ (Cranmer et al., 2015). Neural SBI methods estimate an *amortized* inference network using simulated parameter-data training samples, such that after this initial offline training stage, inference can be done during test-time for new observations cheaply with a single forward pass through the network. In this work, we focus on the canonical neural posterior estimator (NPE) (Papamakarios & Murray, 2016), which learns $q_\psi(\theta | \mathbf{x}) \approx p(\theta | \mathbf{x})$, where ψ are parameters of a neural conditional density estimator. In high-dimensional data spaces, such as when we have a dataset of N i.i.d. observations $\mathbf{x}_{1:N}$, we typically leverage a summary statistic $f : \mathcal{X}^N \rightarrow \mathcal{S}$ and perform inference on the summary space $q_\psi(\theta | \mathbf{s})$ where $\mathbf{s} = f(\mathbf{x}_{1:N})$. This summary statistic can either be hand-crafted (Fearnhead & Prangle, 2012), or learned with a neural encoder (Chen et al., 2020). Concretely, NPE uses training samples $\{(\theta^{(i)}, \mathbf{x}_{1:N}^{(i)}, \mathbf{s}^{(i)})\}_{i=1}^M$, $\mathbf{s} = f(\mathbf{x}_{1:N})$ that are drawn from the following generative process: $\theta \sim \pi(\theta)$, $\mathbf{x}_{1:N} \sim p_\theta(\mathbf{x}_{1:N})$ and $\mathbf{s} = f(\mathbf{x}_{1:N})$. Then, the NPE is trained by minimizing the negative log-likelihood loss $\mathcal{L}(\psi) = -\frac{1}{M} \sum_{i=1}^M \log q_\psi(\theta^{(i)} | \mathbf{s}^{(i)})$.

Beyond amortizing inference across observations, there has been a recent trend towards general-purpose inference engines, where pretrained models are reused across a wide range of inference tasks and setups. These include all-in-one models representing different conditional distributions of the joint simulator distribution (Gloeckler et al., 2024), training-free approaches (Vetter et al., 2025) leveraging probabilistic

foundation models (Müller et al.), and test-time procedures adapting amortized models to new priors (Yang et al., 2025).

2.2. Robust simulation-based inference

Model misspecification arises when the data-generating distribution $\tilde{\mathbb{P}}$ lies outside of the simulator model family $\{\mathbb{P}_\theta : \theta \in \Theta\}$. In neural SBI, this is a particularly acute issue due to the additional model approximation from neural density estimation, and even a moderate mismatch has been shown to affect the accuracy and calibration of resulting posteriors (Ward et al., 2022; Cannon et al., 2022). Because the NPE is estimated from training samples, the distribution of training samples plays a key role in determining the effects of model misspecification, which is the prior-predictive distribution $m(\mathbf{x}_{1:N}) = \int \left(\prod_{n=1}^N p(\mathbf{x}_n | \theta) \right) \pi(\theta) d\theta$.

This dependence can be made more explicitly by considering the negative log-likelihood objective function of the NPE, which can be shown to be equivalent to (up to additive constants) to,

$$\mathbb{E}_{m(\mathbf{x}_{1:N})} \text{KL}[p(\theta | f(\mathbf{x}_{1:N})), q_\psi(\theta | f(\mathbf{x}_{1:N}))]$$

which is the expected KL-divergence between the true posterior and the NPE, under the prior-predictive distribution. Thus, when the observed data distribution deviates from the prior-predictive distribution, the quality of the NPE deteriorates. The difference between the DGP and the prior-predictive distribution, $\mathcal{D}[m(\mathbf{x}_{1:N}), \tilde{\mathbb{P}}(\mathbf{x}_{1:N})]$ is thus known as the simulation gap (Schmitt et al., 2024).

There has been a growing literature of robust SBI approaches that have been developed in order to tackle model misspecification. Following the taxonomy in Kelly et al. (2025), existing approaches can be broadly grouped into three classes: (i) *robust summary approaches* that construct summary statistics that remove aspects of the data responsible for misspecification (Huang et al., 2023), (ii) *generalized Bayesian methods* that modifies the likelihood in the standard Bayesian update rule with a robust loss or divergence (Bissiri et al., 2016; Dellaporta et al., 2022) and (iii) *error modeling* which introduces an explicit error model to account for the gap between simulations and observed data (Ratmann et al., 2009; Frazier & Drovandi, 2021). Although these approaches are effective, many methods inherently couple robustness to the inference engine and limit amortization, such as requiring observations during joint training with the NPE (Huang et al., 2023; Elsemüller et al., 2025) or additional error models (Ward et al., 2022; Kelly et al., 2024).

2.3. Maximum mean discrepancy based inference

The maximum mean discrepancy (MMD) (Gretton et al., 2012) is a kernel-based discrepancy between two distribu-

tions \mathbb{P}, \mathbb{Q} on \mathcal{X} , defined with respect to a positive definite kernel $k : \mathcal{X} \times \mathcal{X} \rightarrow \mathbb{R}$ and its reproducing kernel Hilbert space (RKHS) \mathcal{H} . Let $\phi : \mathcal{X} \rightarrow \mathcal{H}$ be a feature map such that $k(\mathbf{x}, \mathbf{y}) = \langle \phi(\mathbf{x}), \phi(\mathbf{y}) \rangle_{\mathcal{H}}$. The kernel mean embedding of \mathbb{P} is $\mu_{\mathbb{P}} = \mathbb{E}_{\mathbf{x} \sim \mathbb{P}}[k(\mathbf{x}, \cdot)] = \mathbb{E}_{\mathbf{x} \sim \mathbb{P}}[\phi(\mathbf{x})]$ (Muandet et al., 2017), and the MMD is defined based on the distance between mean embeddings in the RKHS: $\text{MMD}(\mathbb{P}, \mathbb{Q}) = \|\mu_{\mathbb{P}} - \mu_{\mathbb{Q}}\|_{\mathcal{H}}$. When the kernel is bounded, the MMD objective can be shown to have robustness properties under contamination (Chérief-Abdellatif & Alquier, 2022). Motivated by the computational complexity of the MMD, random Fourier features (Rahimi & Recht, 2007) are an approximation to shift-invariant kernels using a finite-dimensional feature map $\mathbf{z} : \mathcal{X} \rightarrow \mathbb{R}^D$, allowing us to approximate the MMD as $\text{MMD}(\mathbb{P}, \mathbb{Q}) \approx \|\mathbb{E}_{\mathbf{x} \sim \mathbb{P}}[\mathbf{z}(\mathbf{x})] - \mathbb{E}_{\mathbf{x} \sim \mathbb{Q}}[\mathbf{z}(\mathbf{x})]\|_2$.

The MMD can be estimated directly from samples of the distributions \mathbb{P}, \mathbb{Q} , without requiring density evaluation, making the MMD a naturally well-suited divergence for simulator models. In particular, the MMD has been used for statistical inference of simulator models under the minimum distance estimation framework (Wolfowitz, 1957), and the resulting estimators have been shown to be consistent and robust under misspecification (Briol et al., 2019). MMD-based discrepancies have also been leveraged in approximate Bayesian computation (Park et al., 2016), generalized Bayesian inference (Chérief-Abdellatif & Alquier, 2020; Dellaporta et al., 2022), and more broadly in generative modeling (Li et al., 2015; Dziugaite et al., 2015).

3. Methodology

Recall that our goal is to develop a lightweight test-time procedure for robust SBI, that is fully decoupled from the pretrained neural posterior estimator (NPE). We introduce *minimum-distance summaries* (MDS), which, given test-time observations $\tilde{\mathbf{x}}_{1:N}$, MDS selects an adapted summary \mathbf{s}^* by minimizing the simulation-gap in *data-space*, specifically, we minimize a robust divergence between the summary-conditional data distribution $\mathbb{P}_{\mathbf{x} | \mathbf{s}}$ and the empirical distribution of $\tilde{\mathbf{x}}_{1:N}$. Performing this alignment on data-space leverages robustness directly where misspecification is most interpretable, and crucially, because the NPE depends on observations only through the queried summary \mathbf{s} , the MDS \mathbf{s}^* can be estimated and queried directly into the NPE q_ψ completely independently of the NPE.

3.1. Minimum-distance summaries

Recall that the NPE $q_\psi(\theta | \mathbf{s})$ is trained under the prior-predictive distribution, which is generated from the following generative process, $\theta \sim \pi(\theta)$, $\mathbf{x}_{1:N} | \theta \sim \prod_{n=1}^N p(\mathbf{x}_n | \theta)$, and $\mathbf{s} = f(\mathbf{x}_{1:N})$. As our goal is to minimize the discrepancy in data-space, in order to connect a candidate summary statistic \mathbf{s} to the data distribution, we consider the summary

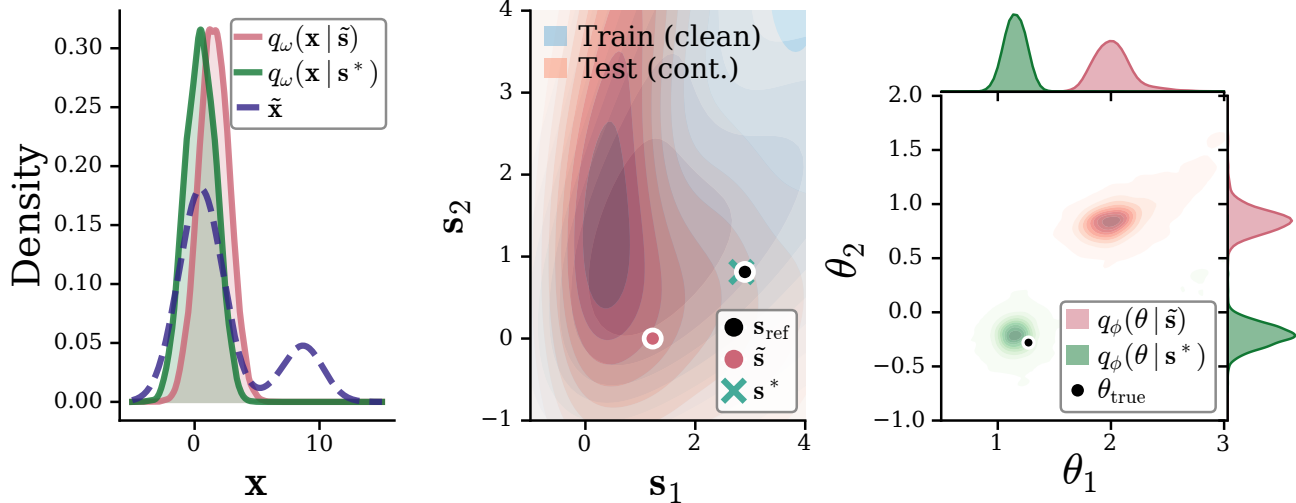


Figure 1. MDS for a bivariate Gaussian model with 20% of observations $\tilde{x}_{1:100}$ contaminated by a shift of 8 units. s_{ref} , \tilde{s} , s^* are the oracle (uncontaminated) summary, test observation (contaminated) summary and adapted MDS summary respectively. Left: MDS aligns the decoder model q_ω with the contaminated observations \tilde{x} using a robust divergence. Middle: MDS is able to recover the oracle summary despite aligning on the data space. Right: MDS robustifies the NPE and the NPE is now able to recover the true parameters.

conditional data distribution $\mathbb{P}_{\mathbf{x}|\mathbf{s}} = \text{Law}(\mathbf{x}_1 \mid S = \mathbf{s}) \in \mathcal{P}(\mathcal{X})$. In particular, note that when $\mathbf{x}_{1:N}$ are i.i.d. samples, and f is a permutation-invariant summary statistic, the conditional distribution $\mathbf{x}_{1:N} \mid S = \mathbf{s}$ is exchangeable over N and consequently, conditional distributions $\text{Law}(\mathbf{x}_n \mid S = \mathbf{s})$ are identical for all n .

Given a target distribution $\mathbb{Q} \in \mathcal{P}(\mathcal{X})$, we define the minimum-distance summary (MDS) as follows:

$$\mathbf{s}^*(\mathbb{Q}) = \arg \min_{\mathbf{s} \in \mathcal{S}} \mathcal{D}(\mathbb{P}_{\mathbf{x}|\mathbf{s}}, \mathbb{Q}), \quad (1)$$

where \mathcal{D} is a statistical divergence between the distributions defined on \mathcal{X} . For an observed dataset $\tilde{\mathbf{x}}_{1:N}$, we take \mathbb{Q} to be the empirical distribution of the observed dataset, $\hat{\mathbb{P}}_N := \frac{1}{N} \sum_{n=1}^N \delta_{\tilde{\mathbf{x}}_n}$. The MDS objective can thus be seen as a projection of the empirical distribution on the family of models $\{\mathbb{P}_{\mathbf{x}|\mathbf{s}} : \mathbf{s} \in \mathcal{S}\}$, analogously to minimum-distance estimation (Wolfowitz, 1957). Intuitively, the MDS \mathbf{s}^* represents the summary statistic that best matches the empirical distribution, under a certain choice of divergence. As we will see in subsequent sections, the choice of divergence is crucial in ensuring robustness and computational efficiency of our MDS. We note here that the MDS objective is defined on *marginal* datapoints, instead of over the entire dataset $\mathbf{x}_{1:N}$, as we only observe a single realization of the observation dataset $\tilde{\mathbf{x}}_{1:N}$, making divergence estimation on this space statistically inefficient.

Amortized decoder estimation Depending on the choice of divergence \mathcal{D} in Equation (1), we require access to some aspect of the summary-conditional data distribution

$\mathbb{P}_{\mathbf{x}|\mathbf{s}}$. We approximate this distribution with an amortized conditional density estimator $q_\omega(\mathbf{x} \mid \mathbf{s})$, trained offline using the same training samples used for NPE training, $\{(\mathbf{x}_{1:N}^{(i)}, \mathbf{s}^{(i)})\}_{i=1}^M$ (allowing us to avoid additional simulations), which we call a *decoder model*, as it inverts the summary statistic back onto marginal data points.

Depending on the type of divergence \mathcal{D} , we may require exact densities, or possibly just samples from the distribution. A flexible choice of neural density estimator would thus be a flow-based model (Papamakarios et al., 2017; Durkan et al., 2019), which allows for both exact density evaluation and sampling. A flow-based conditional density estimator can be used as a decoder model q_ω with training with the negative log-likelihood loss, $\mathcal{L}(\omega) = -\frac{1}{MN} \sum_{i=1}^M \sum_{n=1}^N \log q_\omega(\mathbf{x}_n^{(i)} \mid \mathbf{s}^{(i)})$.

Given the trained, amortized decoder model, during test-time, given observations $\tilde{\mathbf{x}}_{1:N}$, we can estimate the objective in Equation (1) with $\mathcal{D}(q_\omega(\mathbf{x} \mid \mathbf{s}), \hat{\mathbb{P}}_N)$, which can be optimized directly with respect to \mathbf{s} to obtain the MDS. A standard choice of divergence would be the forward KL divergence (Kullback & Leibler, 1951), which is equivalent to likelihood maximization. Since our goal is to obtain a *robust* SBI approach, we require a robust divergence, which makes the KL unsuitable. Instead, a natural choice for a robust divergence would be the maximum-mean discrepancy (MMD). We provide a comparison of this in Appendix B. Furthermore, a computational issue faced with our approach is that the decoder model requires conditional density estimation, which is in general expensive and limits the general applicability of our method. As we shall see in the next section, using the MMD would allow us to solve this com-

putational challenge too, by bypassing the need for full density estimation.

3.2. Maximum mean discrepancy MDS

The maximum mean discrepancy (MMD) (Gretton et al., 2012) is a highly attractive choice of discrepancy \mathcal{D} for MDS estimation as it has strong mathematical properties, in particular being robust under outlier contamination for bounded kernels (Chérief-Abdellatif & Alquier, 2022), and as it depends on distributions only through their kernel mean embeddings, allows us to sidestep density estimation. Inheriting the robustness properties from the MMD, we provide theoretical results on the MMD based MDS in Section 4.

Recall that for two probability distributions $\mathbb{P}, \mathbb{Q} \in \mathcal{P}(\mathcal{X})$, the MMD is defined $\text{MMD}^2(\mathbb{P}, \mathbb{Q}) = \|\mu_{\mathbb{P}} - \mu_{\mathbb{Q}}\|_{\mathcal{H}}^2$ where ϕ is the feature map associated with k , \mathcal{H} is the corresponding RKHS, and $\mu_P := \mathbb{E}_{x \sim \mathbb{P}}[\phi(x)]$ is the kernel mean embedding. Using this in our MDS objective Equation 1,

$$\begin{aligned} \mathbf{s}^* &= \arg \min_{\mathbf{s} \in \mathcal{S}} \text{MMD}^2(\mathbb{P}_{\mathbf{x}|\mathbf{s}}, \hat{\mathbb{P}}_N) \\ &= \arg \min_{\mathbf{s} \in \mathcal{S}} \left\| \mu(\mathbf{s}) - \frac{1}{N} \sum_{n=1}^N \phi(\tilde{\mathbf{x}}_n) \right\|_{\mathcal{H}}^2, \end{aligned}$$

where we have $\mu(\mathbf{s}) := \mathbb{E}[\phi(\mathbf{x}) \mid S = \mathbf{s}]$.

Crucially, note that since the objective depends on the distribution $\mathbb{P}_{\mathbf{x}|\mathbf{s}}$ only through its conditional mean embedding $\mu(\mathbf{s})$. These conditional mean embeddings can then be estimated directly (Song et al., 2009; 2013), but requires a computationally expensive Gram matrix inversion, which is especially problematic if the number of training samples are large.

With the goal of obtaining a fast, lightweight estimation procedure, we leverage random Fourier features (Rahimi & Recht, 2007), which allows us to approximate the Gaussian kernel feature map with a finite dimensional feature map $\mathbf{z}(\cdot) \in \mathbb{R}^K$ based on the Fourier transform of the kernel. Under this approximation, the MDS objective can be further approximated as the Euclidean distance between finite-dimensional mean embeddings,

$$\text{MMD}^2(\mathbb{P}_{\mathbf{x}|\mathbf{s}}, \hat{\mathbb{P}}_N) \approx \left\| \mathbb{E}[\mathbf{z}(\mathbf{x}) \mid S = \mathbf{s}] - \frac{1}{N} \sum_{n=1}^N \mathbf{z}(\tilde{\mathbf{x}}_n) \right\|_2^2 \quad (2)$$

Amortized decoder mean embedding By leveraging the random Fourier feature objective in Equation (2), we can now directly estimate the conditional mean embedding via regression. Specifically, using training samples (from the NPE training) $\{(\bar{\mathbf{z}}^{(i)}, \mathbf{s}^{(i)})\}_{i=1}^M$, where $\bar{\mathbf{z}}^{(i)} =$

$\frac{1}{N} \sum_{n=1}^N \mathbf{z}(\mathbf{x}_n^{(i)})$ is the empirical mean embedding, we can estimate the conditional decoder mean embedding $\mu_{\omega} : \mathbb{R}^{d_s} \rightarrow \mathbb{R}^K$, by simply minimizing a mean-squared error loss function, $\mathcal{L}(\omega) = \frac{1}{M} \sum_{i=1}^M \|\mu_{\omega}(\mathbf{s}^{(i)}) - \bar{\mathbf{z}}^{(i)}\|_2^2$. In practice, we parameterize the decoder mean embedding $\hat{\mu}_{\omega}$ as a neural network, which is particularly suitable for predicting high dimensional random Fourier feature embeddings. In particular, note that, as with the density-based decoder model proposed earlier, the estimated decoder mean embedding $\hat{\mu}(\mathbf{s})$ is amortized with respect to \mathbf{s} , and can be trained in a completely offline setting, without test observations.

Test-time MDS adaptation At test-time, given an observed dataset $\tilde{\mathbf{x}}_{1:N}$ and the estimated amortized decoder mean embedding $\hat{\mu}_{\omega}$, we can directly optimize the MDS objective Equation (2) with $\mathbf{s}^* = \arg \min_{\mathbf{s} \in \mathcal{S}} \|\hat{\mu}_{\omega}(\mathbf{s}) - \frac{1}{N} \sum_{n=1}^N \mathbf{z}(\tilde{\mathbf{x}}_n)\|_2^2$. Compared to the density-based decoder model optimization, this objective is completely deterministic, and allows for the use of fast gradient-based optimization algorithms, e.g., quasi-Newton methods or line search. We leverage the L-BFGS algorithm (Liu & Nocedal, 1989), initialized at the observed summary statistic $\tilde{\mathbf{s}} = f(\tilde{\mathbf{x}}_{1:N})$. The resulting adapted summary is then used directly as input to the pretrained NPE, providing a lightweight, robust, test-time procedure that is fully decoupled from the NPE. We provide the algorithm using stochastic gradient descent (SGD) in Algorithm 1, and an illustration of the MDS with the MMD in Figure 1. Furthermore, in many realistic modeling scenarios, misspecification is not known a-priori. Since our MDS method adapts the query summary starting from the original observed summary, when combined with a calibration based heuristic, we propose a joint procedure that proceeds with the MDS adaptation only when model misspecification is detected, which we discuss in Appendix C.

4. Theory

In this section, we provide theoretical guarantees on the robustness and consistency of the posteriors produced with our proposed minimum-distance summaries (MDS) with the maximum-mean discrepancy (MMD).

4.1. Robustness

We analyze the sensitivity of the posterior distribution obtained by querying with the MDS, under contamination of the target data distribution. We denote $\{\mathbb{P}_{\theta|\mathbf{s}} : \mathbf{s} \in \mathcal{S}\}$ as the family of summary posterior distributions defined on $\mathcal{P}(\Theta)$, and $\{\mathbb{P}_{\mathbf{x}|\mathbf{s}} : \mathbf{s} \in \mathcal{S}\}$ as the family of summary-conditional data distributions defined on $\mathcal{P}(\mathcal{X})$. We assume both families admit regular conditional distributions, for all $\mathbf{s} \in \mathcal{S}$. We note that these conditionals may be exact, or approximations, in our proposed MDS approach they correspond to

Algorithm 1 MMD minimum distance summary with SGD

```

1: Offline (Training-time)
2: Inputs: Training samples  $\{(\mathbf{x}_{1:N}^{(i)}, \mathbf{s}^{(i)})\}_{i=1}^M$ , decoder
   mean embedding model  $\mu_\omega(\mathbf{s})$ 
3: Compute empirical mean embeddings for training sam-
   ples  $\bar{\mathbf{z}}^{(i)} = \frac{1}{N} \sum_{n=1}^N \mathbf{z}(\mathbf{x}_n^{(i)})$ 
4: Estimate decoder mean embedding  $\hat{\mu}_\omega(\mathbf{s})$  with MSE
   objective  $\mathcal{L}(\omega) = \frac{1}{M} \sum_{i=1}^M \|\mu_\omega(\mathbf{s}^{(i)}) - \bar{\mathbf{z}}^{(i)}\|_2^2$ 
5: Return: Decoder mean embedding  $\hat{\mu}_\omega(\mathbf{s})$  (Amortized)
6: Online (Test-time)
7: Inputs: Observations  $\tilde{\mathbf{x}}_{1:N}$ , pretrained NPE  $q_\psi(\theta | \mathbf{s})$ ,
   SGD step size  $\eta$  and iterations  $T$ 
8: Compute empirical mean embeddings for observations
    $\hat{\mu}_{\text{obs}} = \frac{1}{N} \sum_{n=1}^N \mathbf{z}(\tilde{\mathbf{x}}_n)$ 
9: Compute initial summary statistic  $\mathbf{s}_0 \leftarrow f(\tilde{\mathbf{x}}_{1:N})$ 
10: for  $t = 0$  to  $T - 1$  do
11:    $\mathbf{s}_{t+1} \leftarrow \mathbf{s}_t - \eta \cdot \nabla_{\mathbf{s}} \|\hat{\mu}_\omega(\mathbf{s}_t) - \hat{\mu}_{\text{obs}}\|_2^2$ 
12: end for
13:  $\mathbf{s}^* \leftarrow \mathbf{s}_T$ 
14: Return: NPE evaluated at MDS:  $q_\psi(\theta | \mathbf{s}^*)$ 

```

the pretrained NPE q_ψ and decoder model q_ω respectively.

Recall that, given a target distribution $\mathbb{Q} \in \mathcal{P}(\mathcal{X})$, the population MMD based minimum-distance summary objective is:

$$\mathbf{s}^*(\mathbb{Q}) = \arg \min_{\mathbf{s} \in \mathcal{S}} \text{MMD}(\mathbb{P}_{\mathbf{x}|\mathbf{s}}, \mathbb{Q}),$$

where the MMD is computed with respect to a fixed kernel k . We assume a minimizer exists, and refer to Briol et al. (2019) for conditions guaranteeing this.

In order to model outlier contamination, we consider the classic Huber's ϵ contamination model. For any $\mathbf{y} \in \mathcal{X}$ and $\epsilon \in [0, 1]$, define the contaminated distribution $\mathbb{Q}_\epsilon = (1 - \epsilon)\mathbb{Q} + \epsilon\delta_{\mathbf{y}}$. Theorem 4.1 shows that, a small contamination to the target distribution \mathbb{Q} leads to a proportionally small change (as measured by the KL divergence) to the resulting posterior approximation with the MDS.

Theorem 4.1. *Consider any $\mathbb{Q} \in \mathcal{P}(\mathcal{X})$ and $\mathbf{y} \in \mathcal{X}$, and let $\mathbb{Q}_\epsilon = (1 - \epsilon)\mathbb{Q} + \epsilon\delta_{\mathbf{y}}$, for $\epsilon \in [0, 1]$. Then, under the conditions of Appendix A.1:*

$$\text{KL}[\mathbb{P}_{\theta|\mathbf{s}^*(\mathbb{Q})}, \mathbb{P}_{\theta|\mathbf{s}^*(\mathbb{Q}_\epsilon)}] = \mathcal{O}(\epsilon). \quad (3)$$

Proof. See Appendix A.2. □

Proof sketch Our proof is composed of three parts. Firstly, the results of Briol et al. (2019) show that the MDS is stable under contamination, i.e., $\mathbf{s}^*(\mathbb{Q})$ and $\mathbf{s}^*(\mathbb{Q}_\epsilon)$ are close. Secondly, we show that this implies the resulting likelihoods are close. Finally, this lets us leverage the results of Sprungk (2020) to show that the posteriors are close in KL.

4.2. Consistency

We provide a consistency result for the MMD-based minimum-distance summary, showing that, when the model is correctly specified, using the MDS does not affect posterior consistency. Intuitively, if the posterior distribution conditioned on the original summary statistic \mathbf{s}_N concentrates on the true parameter θ_0 as $N \rightarrow \infty$, then the posterior distribution conditioned on the MDS \mathbf{s}^* concentrates in a similar way as well. Note that we use \mathbf{s}_N instead of \mathbf{s} to highlight the dependency on the number of samples in the summary statistic $\mathbf{s}_N = f_N(\mathbf{x}_{1:N})$.

We can now state our result, showing consistency under the original summaries \mathbf{s}_N implies consistency under the minimum distance summaries \mathbf{s}_N^* .

Theorem 4.2. *Under the conditions of Appendix A.3, if $\mathbb{P}_{\theta|\mathbf{s}_N}$ converges weakly to δ_{θ_0} for almost every sequence $(\mathbf{x}_i)_{i \geq 1}$ sampled under θ_0 , then $\mathbb{P}_{\theta|\mathbf{s}_N^*}$ converges weakly to δ_{θ_0} as well.*

Proof. See Appendix A.4 □

Proof sketch The proof shows that the predictive mixture distribution induced by $\mathbb{P}_{\theta|\mathbf{s}_N^*}$ converges to the true data-generating distribution \mathbb{P}_{θ_0} , and then uses a strong identifiability assumption to ensure $\mathbb{P}_{\theta|\mathbf{s}_N^*}$ converges to δ_{θ_0} .

5. Related Works

As discussed in Section 2.2, there is a growing body of robust SBI approaches, and MDS fits most naturally as a *robust summaries* method, but differs in its focus as a lightweight, test-time robustification that preserves amortization. A related line of work minimizes the simulation-gap in the summary-space by introducing a regularization term during joint training of a NPE with a neural summary statistic network (Huang et al., 2023; Elsemüller et al., 2025), which can be framed as a form of unsupervised domain adaptation. In contrast, MDS minimizes the simulation-gap in data-space and preserves amortization by adapting purely on the summary queries. A complementary direction introduces explicit error models to account for the simulation-gap (Ward et al., 2022; Kelly et al., 2024). The robust NPE of Ward et al. (2022) augments NPE with a spike-and-slab error model, and performs inference by integrating over latent variables. While statistically principled, such approaches require additional modeling assumptions and nontrivial test-time computations (additional MCMC over latent variables). Our proposed MDS, by leveraging the MMD, is model-free, and has a lightweight test-time adaptation in the form of a deterministic optimization problem.

6. Numerical Experiments

In this section, we empirically evaluate our proposed minimum-distance summary with the maximum-mean discrepancy, focusing on lightweight decoder mean embedding approach as discussed in Section 3.2. For all experiments, we adopt Huber’s contamination model, where the observed test data $\tilde{x}_{1:N}$ is drawn i.i.d. from $\tilde{\mathbb{P}} = \varepsilon\mathbb{Q} + (1 - \varepsilon)\mathbb{P}_{\theta^*}$, where $\varepsilon \in \{0.0, 0.1, \dots, 0.5\}$, θ^* is the ground-truth parameter and \mathbb{Q} is task-specific contamination. For all experiments presented in this section, we use $N = 100$ i.i.d. observations in the datasets. We focus on tasks with a fixed summary statistic, except for the Gaussian setup in Section 6.1, which uses a learnt neural summary statistic.

Throughout our experiments, we maintain a standard NPE which is used as a non robust baseline. We implement the noisy NPE (NNPE) from Ward et al. (2022), which is based on a spike-and-slab error model, an alternate outlier removal baseline method, which pre-processes test observations with outlier detection, which we call NPE-OR, and finally, for the Gaussian setup, the NPE-RS of Huang et al. (2023); Elsemüller et al. (2025). Further details and additional results of all experiments are provided in Appendix D. We use the misspecification detection calibration scheme as discussed in Appendix C, which we find improves the performance for the well-specified test examples, while still maintaining the robustness from adaptation during contamination. Further ablations with respect to the sample size and data dimension is provided in Appendix D.1.1.

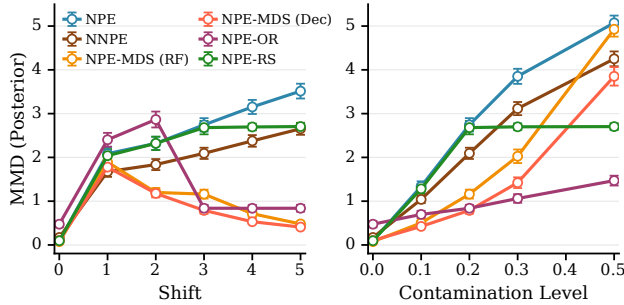


Figure 2. Bivariate Gaussian model with outlier contamination, comparing posterior samples against the groundtruth posterior distribution with MMD. Left: Increasing outlier magnitude. Right: Increasing contamination proportion.

6.1. Gaussian model

We consider a conjugate bivariate Gaussian location model, with a Gaussian prior, which provides an analytic posterior distribution as a ground truth reference distribution. We induce contamination by replacing data points with outliers, with equal probability in both the positive and negative direction, with increasing magnitude of both the outlier points, and the proportion of contamination. We further implement

both the MDS with the full decoder model [*MDS (Dec)*] and MDS with the random Fourier feature based decoder mean embedding [*MDS (RF)*]. From Figure 2, we can see that, in general, our MDS improves robustness compared to other benchmark methods, although for severe proportion of contamination, MDS can degrade. Theoretically, we expect the MDS to be guaranteed only for relatively small levels of contamination. Furthermore, note that on the left plot of Figure 2, we see that there is a sudden drop in NPE-MDS and NPE-OR methods despite increasing outlier shift. We attribute this to the misspecification detection procedure resulting in false negatives for smaller levels of outlier shift. We furthermore evaluate the same task on the NPE-PFN model (Vetter et al., 2025), and show that the MDS can provide test-time robustness in a similar fashion for foundation model-based SBI approaches, which is provided in Appendix D.1.2.

6.2. Time-series examples

We evaluate two time-series models with progressing levels of difficulty based on the dimensionality of the data-space.

Ornstein-Uhlenbeck Process We consider an OUP with a two-dimensional parameter θ and trajectories of length $T = 25$. This follows a similar setup to Huang et al. (2023), but instead of a learned neural summary statistics, we use a fixed summary statistics. The misspecification is induced by contaminating some of the trajectories with samples from a fixed contamination parameter outside of the prior distribution, as well as by increasing the diffusion coefficient in the model. As shown in the top row of Figure 3, MDS-MMD yields consistently improved robustness across contamination levels. Notably, even though the MDS objective minimizes the simulation-gap in the data space, the adapted summary remains close to the clean, uncontaminated observation summary.

SIR Model Next, we consider the SIR model from Ward et al. (2022), with a two-dimensional parameter space and trajectories of length $T = 365$. In this setup, misspecification is structural, where we apply a weekend-reporting delay to the observed time series, producing a systematic discrepancy. With reference to the bottom row of Figure 3, MDS improves upon the standard NPE and NPE-OR, but does not match NNPE. Interestingly, even when the adapted summary deviates from the oracle summary under stronger misspecification, the degradation in posterior metrics is limited, which we attribute to partial non-identifiability of the summary statistic for this model.

6.3. Cryo-EM Inference

Finally, we consider a realistic and challenging simulator model, based on cryo-electron microscopy (cryo-EM) (Din-

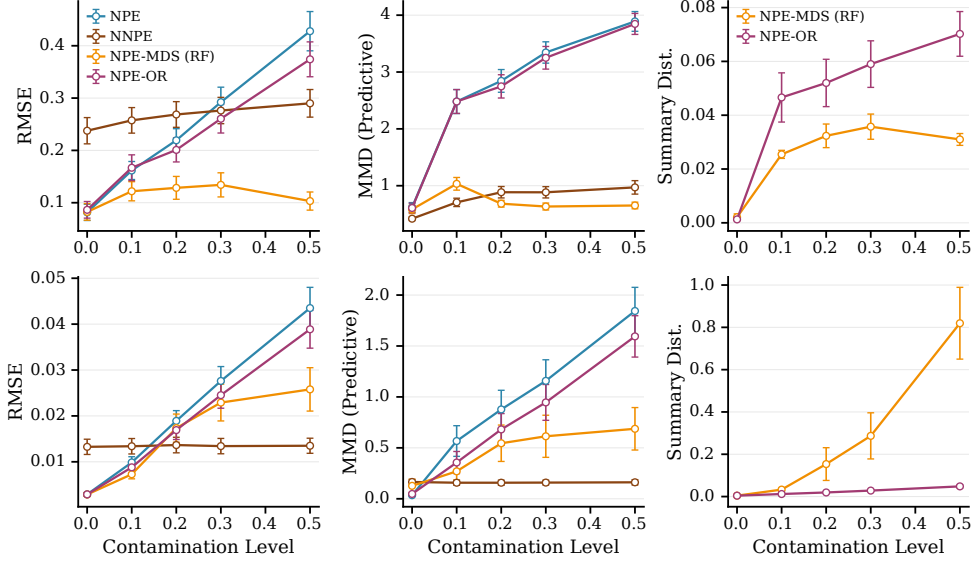


Figure 3. Time-series models with increasing contamination proportion, measuring the RMSE against the true parameter, posterior predictive against uncontaminated observations with MMD, and distance of adapted summary to the uncontaminated (oracle) summary statistic. Top: Ornstein-Uhlenbeck process. Bottom: SIR model.

geldein et al., 2025). Here, each observation is a 32×32 image ($d_x = 1024$) obtained by projecting a 3D biomolecule under unknown orientation, shift, and measurement noise. The goal is to infer a one-dimensional shape index from the image. We induce misspecification by replacing an ε fraction of images in the test observations with Gaussian noise (Figure 5). Despite the high dimensionality and the severe nature of the contamination, MDS is able to substantially improve the robustness of the NPE Figure 4 to contamination.

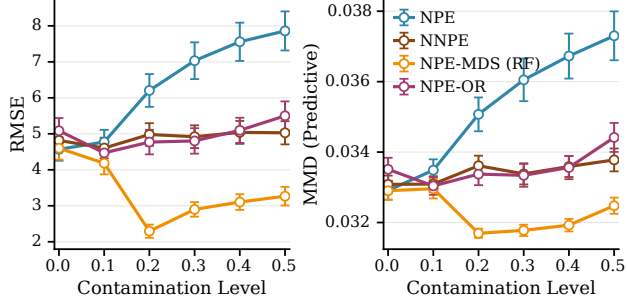


Figure 4. Cryo-EM inference. Left: RMSE against true parameter. Right: Posterior predictive against uncontaminated observations.

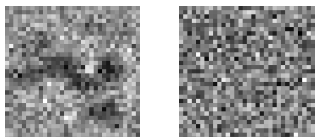


Figure 5. Left: Projected image with HSP90 model. Right: Gaussian noise contamination.

7. Conclusion

We introduced minimum-distance summaries (MDS), a lightweight, test-time robustification procedure for pre-trained NPE. MDS provides an adapted summary by minimizing a *robust* divergence between the data distribution and observations, mitigating misspecification, and crucially, obtains the robust adapted summary independently of the pretrained NPE, decoupling robustness from the inference engine and enabling post-hoc robustification at test-time. Thus, MDS is able to preserve the amortization property of the NPE, providing a modular approach that can be flexibly integrated in a broader statistical workflow. By leveraging the MMD as the divergence, we are able to provide a model-free, lightweight, and robust objective for the MDS. We establish theoretical guarantees of the MDS posterior consistency and stability under contamination. Across a range of synthetic and high-dimensional benchmarks, MDS improves robustness under contamination while maintaining strong performance in the well-specified regime.

Limitations MDS is currently tailored towards inference engines which are queried via a summary, such as the NPE. Extending this query-side adaptation to other amortized engines may require additional modifications to the objective. Since the MDS divergence operates on the data-space, for high-dimensional or structured data, specific choices of MMD kernels or learned feature representation may be necessary. While the MDS is a general framework for any divergence, we focused on the MMD, and an interesting future direction would be to explore problem settings motivating the use of alternate divergences.

Acknowledgements

SK was supported by the EPSRC Center for Doctoral Training in Computational Statistics and Data Science, grant number EP/S023569/1. Thanks to Sam Power for helpful discussions.

Impact Statement

This paper presents work whose goal is to advance the field of Machine Learning. There are many potential societal consequences of our work, none which we feel must be specifically highlighted here.

References

Alsing, J., Charnock, T., Feeney, S., and Wandelt, B. Fast likelihood-free cosmology with neural density estimators and active learning. *Monthly Notices of the Royal Astronomical Society*, pp. stz1960, July 2019. ISSN 0035-8711, 1365-2966. doi: 10.1093/mnras/stz1960. URL <http://arxiv.org/abs/1903.00007>.

Beaumont, M. A., Zhang, W., and Balding, D. J. Approximate Bayesian Computation in Population Genetics. *Genetics*, 162(4):2025–2035, December 2002. ISSN 1943-2631. doi: 10.1093/genetics/162.4.2025. URL <https://doi.org/10.1093/genetics/162.4.2025>.

Bissiri, P. G., Holmes, C. C., and Walker, S. G. A general framework for updating belief distributions. *Journal of the Royal Statistical Society. Series B, Statistical Methodology*, 78(5):1103–1130, November 2016. ISSN 1369-7412. doi: 10.1111/rssb.12158. URL <https://pmc.ncbi.nlm.nih.gov/articles/PMC5082587/>.

Boelts, J., Deistler, M., Gloeckler, M., Álvaro Tejero-Cantero, Lueckmann, J.-M., Moss, G., Steinbach, P., Moreau, T., Muratore, F., Linhart, J., Durkan, C., Vetter, J., Miller, B. K., Herold, M., Ziaeemehr, A., Pals, M., Gruner, T., Bischoff, S., Krouglova, N., Gao, R., Lappalainen, J. K., Mucsányi, B., Pei, F., Schulz, A., Stefanidi, Z., Rodrigues, P., Schröder, C., Zaid, F. A., Beck, J., Kapoor, J., Greenberg, D. S., Gonçalves, P. J., and Macke, J. H. sbi reloaded: a toolkit for simulation-based inference workflows. *Journal of Open Source Software*, 10(108):7754, 2025. doi: 10.21105/joss.07754. URL <https://doi.org/10.21105/joss.07754>.

Briol, F.-X., Barp, A., Duncan, A. B., and Girolami, M. Statistical Inference for Generative Models with Maximum Mean Discrepancy, June 2019. URL <http://arxiv.org/abs/1906.05944>.

Cannon, P., Ward, D., and Schmon, S. M. Investigating the Impact of Model Misspecification in Neural Simulation-based Inference, September 2022. URL <http://arxiv.org/abs/2209.01845>.

Chen, Y., Zhang, D., Gutmann, M., Courville, A., and Zhu, Z. Neural approximate sufficient statistics for implicit models. *arXiv preprint arXiv:2010.10079*, 2020.

Cherief-Abdellatif, B.-E. and Alquier, P. MMD-Bayes: Robust Bayesian Estimation via Maximum Mean Discrepancy. In *Proceedings of The 2nd Symposium on Advances in Approximate Bayesian Inference*, pp. 1–21. PMLR, February 2020. URL <https://proceedings.mlr.press/v118/cherief-abdellatif20a.html>.

Cherief-Abdellatif, B.-E. and Alquier, P. Finite sample properties of parametric MMD estimation: Robustness to misspecification and dependence. *Bernoulli*, 28(1), February 2022. ISSN 1350-7265. doi: 10.3150/21-BEJ1338. URL <http://arxiv.org/abs/1912.05737>.

Cranmer, K., Pavez, J., and Louppe, G. Approximating likelihood ratios with calibrated discriminative classifiers. *arXiv preprint arXiv:1506.02169*, 2015.

Cranmer, K., Brehmer, J., and Louppe, G. The frontier of simulation-based inference. *Proceedings of the National Academy of Sciences*, 117(48):30055–30062, December 2020. doi: 10.1073/pnas.1912789117. URL <https://www.pnas.org/doi/10.1073/pnas.1912789117>.

Deistler, M., Boelts, J., Steinbach, P., Moss, G., Moreau, T., Gloeckler, M., Rodrigues, P. L. C., Linhart, J., Lappalainen, J. K., Miller, B. K., Gonçalves, P. J., Lueckmann, J.-M., Schröder, C., and Macke, J. H. Simulation-based inference: A practical guide, 2025. URL <https://arxiv.org/abs/2508.12939>.

Dellaporta, C., Knoblauch, J., Damoulas, T., and Briol, F.-X. Robust Bayesian Inference for Simulator-based Models via the MMD Posterior Bootstrap. In *Proceedings of The 25th International Conference on Artificial Intelligence and Statistics*, pp. 943–970. PMLR, May 2022. URL <https://proceedings.mlr.press/v151/dellaporta22a.html>.

Dingeldein, L., Silva-Sánchez, D., Evans, L., D’Imprima, E., Grigorieff, N., Covino, R., and Cossio, P. Amortized template matching of molecular conformations from cryoelectron microscopy images using simulation-based inference. *Proceedings of the National Academy of Sciences*, 122(23):e2420158122, June 2025. doi: 10.1073/pnas.2420158122. URL <https://www.pnas.org/doi/10.1073/pnas.2420158122>.

Dudley, R. M. *Real Analysis and Probability*. Chapman and Hall/CRC, New York, February 2018. ISBN 978-1-351-07619-7. doi: 10.1201/9781351076197.

Durkan, C., Bekasov, A., Murray, I., and Papamakarios, G. Neural spline flows. In *Proceedings of the 33rd International Conference on Neural Information Processing Systems*, number 675, pp. 7511–7522. Curran Associates Inc. URL <https://dl.acm.org/doi/10.5555/3454287.3454962>.

Durkan, C., Bekasov, A., Murray, I., and Papamakarios, G. Neural spline flows. *Advances in neural information processing systems*, 32, 2019.

Dziugaite, G. K., Roy, D. M., and Ghahramani, Z. Training generative neural networks via maximum mean discrepancy optimization. In *Proceedings of the Thirty-First Conference on Uncertainty in Artificial Intelligence*, UAI’15, pp. 258–267, Arlington, Virginia, USA, July 2015. AUAI Press. ISBN 978-0-9966431-0-8.

Elsemüller, L., Pratz, V., von Krause, M., Voss, A., Bürkner, P.-C., and Radev, S. T. Does Unsupervised Domain Adaptation Improve the Robustness of Amortized Bayesian Inference? A Systematic Evaluation. *Transactions on Machine Learning Research*, May 2025. ISSN 2835-8856. URL <https://openreview.net/forum?id=ewgLuvnEw6>.

Evans, L., Murad, O.-V., Dingeldein, L., Cossio, P., Covino, R., and Meila, M. Cryo-EM Images are Intrinsically Low Dimensional. *PRX Life*, 3(3):033025, September 2025. doi: 10.1103/txrb-fw3z. URL <https://link.aps.org/doi/10.1103/txrb-fw3z>.

Fearnhead, P. and Prangle, D. Constructing summary statistics for approximate Bayesian computation: Semi-automatic approximate Bayesian computation. *Journal of the Royal Statistical Society Series B*, 74(3):419–474, 2012. URL <https://ideas.repec.org/a/bla/jorssb/v74y2012i3p419-474.html>.

Frazier, D. T. and Drovandi, C. Robust approximate Bayesian inference with synthetic likelihood. *Journal of Computational and Graphical Statistics*, 30(4):958–976, 2021. ISSN 1061-8600. doi: 10.1080/10618600.2021.1875839. URL <https://research.monash.edu/en/publications/robust-approximate-bayesian-inference-with-synthetic-likelihood>.

Gao, R., Deistler, M., and Macke, J. H. Generalized bayesian inference for scientific simulators via amortized cost estimation. *Advances in Neural Information Processing Systems*, 36:80191–80219, 2023.

Gelman, A., Vehtari, A., Simpson, D., Margossian, C. C., Carpenter, B., Yao, Y., Kennedy, L., Gabry, J., Bürkner, P.-C., and Modrák, M. Bayesian Workflow, November 2020. URL <http://arxiv.org/abs/2011.01808>.

Gloeckler, M., Deistler, M., Weilbach, C. D., Wood, F., and Macke, J. H. All-in-one simulation-based inference. In *Proceedings of the 41st International Conference on Machine Learning*, pp. 15735–15766. PMLR, July 2024. URL <https://proceedings.mlr.press/v235/gloeckler24a.html>.

Gretton, A., Borgwardt, K. M., Rasch, M. J., Schölkopf, B., and Smola, A. A Kernel Two-Sample Test. *Journal of Machine Learning Research*, 13(25):723–773, 2012. ISSN 1533-7928. URL <http://jmlr.org/papers/v13/gretton12a.html>.

Hermans, J., Begy, V., and Louppe, G. Likelihood-free mcmc with amortized approximate ratio estimators. In *International conference on machine learning*, pp. 4239–4248. PMLR, 2020.

Huang, D., Bharti, A., Souza, A., Acerbi, L., and Kaski, S. Learning Robust Statistics for Simulation-based Inference under Model Misspecification. *Advances in Neural Information Processing Systems*, 36:7289–7310, December 2023. URL https://proceedings.neurips.cc/paper_files/paper/2023/hash/16c5b4102a6b6eb061e502ce6736ad8a-Abstract-Confere.html.

Kelly, R. P., Nott, D. J., Frazier, D. T., Warne, D. J., and Drovandi, C. Misspecification-robust sequential neural likelihood for simulation-based inference. *Transactions on Machine Learning Research*, 2024:1–37, 2024.

Kelly, R. P., Warne, D. J., Frazier, D. T., Nott, D. J., Gutmann, M. U., and Drovandi, C. Simulation-based Bayesian inference under model misspecification, March 2025. URL <http://arxiv.org/abs/2503.12315>.

Kingma, D. P. and Ba, J. Adam: A Method for Stochastic Optimization. In Bengio, Y. and LeCun, Y. (eds.), *3rd International Conference on Learning Representations, ICLR 2015, San Diego, CA, USA, May 7-9, 2015, Conference Track Proceedings*. URL <http://arxiv.org/abs/1412.6980>.

Kullback, S. and Leibler, R. A. On information and sufficiency. *The annals of mathematical statistics*, 22(1):79–86, 1951.

Li, Y., Swersky, K., and Zemel, R. Generative moment matching networks. In *Proceedings of the 32nd International Conference on International Conference on Ma*

chine Learning - Volume 37, ICML'15, pp. 1718–1727, Lille, France, July 2015. JMLR.org.

Liu, D. C. and Nocedal, J. On the limited memory bfgs method for large scale optimization. *Mathematical programming*, 45(1):503–528, 1989.

Lueckmann, J.-M., Goncalves, P. J., Bassetto, G., Öcal, K., Nonnenmacher, M., and Macke, J. H. Flexible statistical inference for mechanistic models of neural dynamics. *Advances in neural information processing systems*, 30, 2017.

Marin, J.-M., Pudlo, P., Robert, C. P., and Ryder, R. J. Approximate Bayesian computational methods. *Statistics and Computing*, 22(6):1167–1180, November 2012. ISSN 1573-1375. doi: 10.1007/s11222-011-9288-2. URL <https://doi.org/10.1007/s11222-011-9288-2>.

Muandet, K., Fukumizu, K., Sriperumbudur, B., and Schölkopf, B. Kernel Mean Embedding of Distributions: A Review and Beyond. *Found. Trends Mach. Learn.*, 10(1-2):1–141, June 2017. ISSN 1935-8237. doi: 10.1561/2200000060. URL <https://doi.org/10.1561/2200000060>.

Müller, S., Reuter, A., Hollmann, N., Rügamer, D., and Hutter, F. Position: The Future of Bayesian Prediction Is Prior-Fitted. URL <http://arxiv.org/abs/2505.23947>.

Papamakarios, G. and Murray, I. Fast \epsilon-free Inference of Simulation Models with Bayesian Conditional Density Estimation. In *Advances in Neural Information Processing Systems*, volume 29. Curran Associates, Inc., 2016. URL <https://proceedings.neurips.cc/paper/2016/hash/6aca97005c68f1206823815f66102863-Abstract.html>.

Papamakarios, G., Pavlakou, T., and Murray, I. Masked autoregressive flow for density estimation. *Advances in neural information processing systems*, 30, 2017.

Papamakarios, G., Sterratt, D., and Murray, I. Sequential neural likelihood: Fast likelihood-free inference with autoregressive flows. In *The 22nd international conference on artificial intelligence and statistics*, pp. 837–848. PMLR, 2019.

Park, M., Jitkrittum, W., and Sejdinovic, D. K2-ABC: Approximate Bayesian Computation with Kernel Embeddings. In *Proceedings of the 19th International Conference on Artificial Intelligence and Statistics*, pp. 398–407. PMLR, May 2016. URL <https://proceedings.mlr.press/v51/park16.html>.

Paszke, A., Gross, S., Massa, F., Lerer, A., Bradbury, J., Chanan, G., Killeen, T., Lin, Z., Gimelshein, N., Antiga, L., Desmaison, A., Köpf, A., Yang, E., DeVito, Z., Raison, M., Tejani, A., Chilamkurthy, S., Steiner, B., Fang, L., Bai, J., and Chintala, S. PyTorch: An imperative style, high-performance deep learning library. In *Proceedings of the 33rd International Conference on Neural Information Processing Systems*, number 721, pp. 8026–8037. Curran Associates Inc. URL <https://doi.acm.org/doi/10.5555/3454287.3455008>.

Pedregosa, F., Varoquaux, G., Gramfort, A., Michel, V., Thirion, B., Grisel, O., Blondel, M., Prettenhofer, P., Weiss, R., Dubourg, V., Vanderplas, J., Passos, A., Cournapeau, D., Brucher, M., Perrot, M., and Duchesnay, E. Scikit-learn: Machine Learning in Python. 12:2825–2830. ISSN 1532-4435. URL <https://doi.acm.org/doi/10.5555/1953048.2078195>.

Rahimi, A. and Recht, B. Random Features for Large-Scale Kernel Machines. In *Advances in Neural Information Processing Systems*, volume 20. Curran Associates, Inc., 2007. URL https://papers.nips.cc/paper_files/paper/2007/hash/013a006f03dbc5392effeb8f18fda755-Abstract.html.

Ratmann, O., Andrieu, C., Wiuf, C., and Richardson, S. Model criticism based on likelihood-free inference, with an application to protein network evolution. *Proceedings of the National Academy of Sciences of the United States of America*, 106(26):10576–10581, June 2009. ISSN 1091-6490. doi: 10.1073/pnas.0807882106.

Schmitt, M., Bürkner, P.-C., Köthe, U., and Radev, S. T. Detecting Model Misspecification in Amortized Bayesian Inference with Neural Networks: An Extended Investigation, June 2024. URL <http://arxiv.org/abs/2406.03154>.

Schölkopf, B., Platt, J. C., Shawe-Taylor, J., Smola, A. J., and Williamson, R. C. Estimating the Support of a High-Dimensional Distribution. 13(7):1443–1471. ISSN 0899-7667. doi: 10.1162/089976601750264965. URL <https://doi.org/10.1162/089976601750264965>.

Simon-Gabriel, C.-J., Barp, A., Schölkopf, B., and Mackey, L. Metrizing Weak Convergence with Maximum Mean Discrepancies. *Journal of Machine Learning Research*, 24(184):1–20, 2023. ISSN 1533-7928. URL <http://jmlr.org/papers/v24/21-0599.html>.

Song, L., Huang, J., Smola, A., and Fukumizu, K. Hilbert space embeddings of conditional distributions with applications to dynamical systems. In *Proceedings of the 26th Annual International Conference on Machine Learning*, ICML '09, pp. 961–968, New York, NY,

USA, June 2009. Association for Computing Machinery. ISBN 978-1-60558-516-1. doi: 10.1145/1553374.1553497. URL <https://dl.acm.org/doi/10.1145/1553374.1553497>.

Song, L., Fukumizu, K., and Gretton, A. Kernel embeddings of conditional distributions: A unified kernel framework for nonparametric inference in graphical models. *IEEE Signal Processing Magazine*, 30(4):98–111, 2013.

Sprungk, B. On the local Lipschitz stability of Bayesian inverse problems. *Inverse Problems*, 36(5):055015, April 2020. ISSN 0266-5611. doi: 10.1088/1361-6420/ab6f43. URL <https://doi.org/10.1088/1361-6420/ab6f43>.

Vetter, J., Gloeckler, M., Gedon, D., and Macke, J. H. Effortless, Simulation-Efficient Bayesian Inference using Tabular Foundation Models, October 2025. URL <http://arxiv.org/abs/2504.17660>.

Ward, D., Cannon, P., Beaumont, M., Fasiolo, M., and Schmon, S. Robust Neural Posterior Estimation and Statistical Model Criticism. *Advances in Neural Information Processing Systems*, 35:33845–33859, December 2022. URL https://papers.nips.cc/paper_files/paper/2022/hash/db0eac6747e3631eb91095cd76065611-Abstract-Conference.html.

Wolfowitz, J. The Minimum Distance Method. *The Annals of Mathematical Statistics*, 28(1):75–88, March 1957. ISSN 0003-4851, 2168-8990. doi: 10.1214/aoms/1177707038. URL <https://projecteuclid.org/journals/annals-of-mathematical-statistics/volume-28/issue-1/The-Minimum-Distance-Method/10.1214/aoms/1177707038.full>.

Yang, Y., Rissanen, S., Chang, P. E., Loka, N., Huang, D., Solin, A., Heinonen, M., and Acerbi, L. PriorGuide: Test-Time Prior Adaptation for Simulation-Based Inference, October 2025. URL <http://arxiv.org/abs/2510.13763>.

A. Assumptions and proofs for Theorem 4.1 and 4.2

The main paper uses the notation \mathbb{P}_θ for the distribution of \mathbf{x} under a particular choice of θ . In this appendix we instead write $\mathbb{P}_{\mathbf{x}|\theta}$. This is to make it more obvious which distribution this refers to, and to be consistent with notation for other conditional distributions.

A.1. Assumptions for Theorem 4.1 (robustness)

First we have assumptions to use results from [Sprungk \(2020\)](#).

1. $\mathbb{P}_{\theta|\mathbf{s}}$ has a Lebesgue density proportional to $\pi(\theta) \exp[-\Phi_{\mathbf{s}}(\theta)]$ where $\Phi_{\mathbf{s}} : \Theta \rightarrow \mathbb{R}$ (negative log-likelihood function).
2. For any $\mathbf{s} \in \mathcal{S}$, $\text{ess inf}_\mu \Phi_{\mathbf{s}} = 0$, where μ is the prior measure.

We introduce assumptions on the sensitivity of the log-likelihood to \mathbf{s} .

3. For any $\theta \in \Theta$, $\Phi_{\mathbf{s}}(\theta)$ is a differentiable function in \mathbf{s} . Let $h(\mathbf{t}, \theta) = \nabla_{\mathbf{s}} \Phi_{\mathbf{s}}(\theta)|_{\mathbf{s}=\mathbf{t}}$.
4. For any compact $K \subseteq \mathcal{S}$ there exists $g_K(\theta)$ such that $\sup_{\mathbf{t} \in K} \|h(\mathbf{t}, \theta)\| \leq g_K(\theta)$ and $\int g_K(\theta) \pi(\theta) d\theta < \infty$.

Next we state assumptions to use Theorem 5 of [Briol et al. \(2019\)](#). These are modified to relate to $\mathbb{P}_{\mathbf{x}|\mathbf{s}}$, rather than $\mathbb{P}_{\mathbf{x}|\theta}$ as in [Briol et al. \(2019\)](#).

5. The MMD kernel k has bounded partial derivative in its first argument.
6. $\mathbb{P}_{\mathbf{x}|\mathbf{s}}$ is a pushforward measure $G_{\mathbf{s}}^\# \mathcal{U}$ where $(\mathcal{U}, \mathcal{F}, \mathbb{U})$ is a probability measure and $G_{\mathbf{s}} : \mathcal{U} \rightarrow \mathcal{X}$ is measurable.
7. For all $\mathbf{u} \in \mathcal{U}$, $G_{\mathbf{s}}(\mathbf{u})$ is a continuously differentiable function in \mathbf{s} .
8. For all $\mathbf{s} \in \mathcal{S}$, $\|\nabla_{\mathbf{s}} G_{\mathbf{s}}(\cdot)\| \in L^1(\mathbb{U})$.

A final assumption follows.

9. The summary statistic space \mathcal{S} is convex.

A.2. Proof of Theorem 4.1 (robustness)

For $\mathbf{s}, \mathbf{t} \in \mathcal{S}$, consider

$$\|\Phi_{\mathbf{s}}(\theta) - \Phi_{\mathbf{t}}(\theta)\|_{L^1_\mu} = \int |\Phi_{\mathbf{s}}(\theta) - \Phi_{\mathbf{t}}(\theta)| \pi(\theta) d\theta.$$

By the mean value theorem, $\Phi_{\mathbf{s}}(\theta) - \Phi_{\mathbf{t}}(\theta) = (\mathbf{s} - \mathbf{t})^T h(\mathbf{u}(\theta), \theta)$, where $\mathbf{u}(\theta) = a(\theta)\mathbf{s} + [1 - a(\theta)]\mathbf{t}$ for some $a : \Theta \rightarrow [0, 1]$. By assumption 9, $\mathbf{u}(\theta) \in \mathcal{S}$. Then

$$\|\Phi_{\mathbf{s}}(\theta) - \Phi_{\mathbf{t}}(\theta)\|_{L^1_\mu} \leq \|\mathbf{s} - \mathbf{t}\| \int \|h(\mathbf{u}(\theta), \theta)\| \pi(\theta) d\theta. \quad (4)$$

Consider $\mathbf{t} \in K(\mathbf{s}) = \{\mathbf{t} : \|\mathbf{s} - \mathbf{t}\| \leq 1\}$. By assumption 4, the integral in (4) is finite, so

$$\|\Phi_{\mathbf{s}}(\theta) - \Phi_{\mathbf{t}}(\theta)\|_{L^1_\mu} \leq k_1(\mathbf{s}) \|\mathbf{s} - \mathbf{t}\| \quad (5)$$

for some $k_1 : \mathcal{S} \rightarrow \mathbb{R}$.

Under assumptions 1–2, we can apply Theorem 11 of [Sprungk \(2020\)](#)¹ to get

$$\text{KL}[\mathbb{P}_{\theta|\mathbf{s}}, \mathbb{P}_{\theta|\mathbf{t}}] \leq k_2(\mathbf{s}) \|\Phi_{\mathbf{s}}(\theta) - \Phi_{\mathbf{t}}(\theta)\|_{L^1_\mu} \quad (6)$$

¹The theorem gives (in our notation) a factor $k_2(\mathbf{s}, \mathbf{t})$. Equation (4) of [Sprungk \(2020\)](#) and the surrounding discussion shows how this translates into $k_2(\mathbf{s})$ for a suitable set of \mathbf{t} values.

for some $k_2 : \mathcal{S} \rightarrow \mathbb{R}$, when $\|\Phi_{\mathbf{s}}(\theta) - \Phi_{\mathbf{t}}(\theta)\|_{L^1_\mu} \leq 1$.

Under conditions 5–8, Theorem 5 of Briol et al. (2019) gives:

$$\lim_{\epsilon \rightarrow 0} \frac{1}{\epsilon} \|\mathbf{s}^*(\mathbb{Q}) - \mathbf{s}^*(\mathbb{Q}_\epsilon)\| < \infty. \quad (7)$$

Hence for ϵ sufficiently small we have $\|\mathbf{s}^*(\mathbb{Q}) - \mathbf{s}^*(\mathbb{Q}_\epsilon)\| < 1$ and, by (5), $\|\Phi_{\mathbf{s}^*(\mathbb{Q})}(\theta) - \Phi_{\mathbf{s}^*(\mathbb{Q}_\epsilon)}(\theta)\|_{L^1_\mu} \leq 1$. Then we get

$$\begin{aligned} \frac{1}{\epsilon} \text{KL}[\mathbb{P}_{\theta|\mathbf{s}^*(\mathbb{Q})}, \mathbb{P}_{\theta|\mathbf{s}^*(\mathbb{Q}_\epsilon)}] &\leq k_2(\mathbf{s}^*(\mathbb{Q})) \frac{1}{\epsilon} \|\Phi_{\mathbf{s}^*(\mathbb{Q})}(\theta) - \Phi_{\mathbf{s}^*(\mathbb{Q}_\epsilon)}(\theta)\|_{L^1_\mu} && \text{by (6)} \\ &\leq k_1(\mathbf{s}^*(\mathbb{Q})) k_2(\mathbf{s}^*(\mathbb{Q})) \frac{1}{\epsilon} \|\mathbf{s}^*(\mathbb{Q}) - \mathbf{s}^*(\mathbb{Q}_\epsilon)\| && \text{by (5)} \\ \Rightarrow \quad \lim_{\epsilon \rightarrow 0} \frac{1}{\epsilon} \text{KL}[\mathbb{P}_{\theta|\mathbf{s}^*(\mathbb{Q})}, \mathbb{P}_{\theta|\mathbf{s}^*(\mathbb{Q}_\epsilon)}] &< \infty && \text{by (7)} \end{aligned}$$

as required.

A.3. Assumptions for Theorem 4.2 (consistency)

We assume:

1. The MMD kernel k is bounded, continuous and integrally strictly positive definite (Simon-Gabriel et al., 2023).
2. $\mathbb{P}_{\mathbf{x}|\theta}$ is a pushforward measure $G_\theta^\# \mathcal{U}$ where $(\mathcal{U}, \mathcal{F}, \mathbb{U})$ is a probability measure and $G_\theta : \mathcal{U} \rightarrow \mathcal{X}$ is measurable.
3. For all $u \in \mathcal{U}$, $G_\theta(u)$ is a continuous function in θ .
4. Consider the sequence $\mathbb{T}_N \in \mathcal{P}(\theta)$ and the resulting mixture distributions $\mathbb{Q}_N(A) = \int \mathbb{P}_{\mathbf{x}|\theta}(A) d\mathbb{T}_N$. If \mathbb{Q}_N weakly converges to $\mathbb{P}_{\mathbf{x}|\theta_0}$, then \mathbb{T}_N weakly converges to δ_{θ_0} .

Remark A.1. Assumption 1 ensures that MMD metrizes weak convergence (see Simon-Gabriel et al., 2023, Theorem 1). That is, \mathbb{V}_N weakly converges to \mathbb{V} if and only $\text{MMD}(\mathbb{V}_N, \mathbb{V}) \rightarrow 0$, where the sequence \mathbb{V}_N and \mathbb{V} are in $\mathcal{P}(\mathcal{X})$.

A.4. Proof of Theorem 4.2 (consistency)

We prove this in a particular setting. Consider a parametric family $\mathbb{P}_\theta \in \mathcal{P}(\mathcal{X})$ for $\theta \in \Theta$. Suppose that we have independent random variables $\mathbf{x}_i \sim \mathbb{P}_{\theta_0}$ for $i \in \mathbb{N}_0$ and some true parameter value $\theta_0 \in \Theta$. Given N , we treat $\mathbf{x}_{1:N}$ as observable, and \mathbf{x}_0 as a separate test variable. Let $\hat{\mathbb{P}}_N$ be the empirical distribution $\frac{1}{N} \sum_{i=1}^N \delta_{\mathbf{x}_i}$. Let $\mathbf{s}_N = f_N(\mathbf{x}_{1:N})$ where $f_N : \mathcal{X}^n \rightarrow \mathcal{S}$.

For all N , our setting gives regular conditional distributions $\mathbb{P}_{\theta|\mathbf{s}}^N \in \mathcal{P}(\Theta)$ (summary posterior), and $\mathbb{P}_{\mathbf{x}_0|\mathbf{s}}^N \in \mathcal{P}(\mathcal{X})$ (predictive decoder). These are the exact distributions given the random variables introduced above. This result does not consider approximation error.

The superscripts denote the dependence of these conditional distributions on N .

Define:

$$\mathbf{s}_N^* = \arg \min_{\mathbf{s} \in \mathcal{S}} \text{MMD}(\mathbb{P}_{\mathbf{x}_0|\mathbf{s}}^N, \hat{\mathbb{P}}_N).$$

We assume that this $\arg \min$ exists (as before, see Briol et al. (2019) for conditions guaranteeing this).

We will need two weak convergence requirements²

$$\mathbb{P}_{\theta|\mathbf{s}_N} \rightarrow \delta_{\theta_0}, \quad (8)$$

$$\hat{\mathbb{P}}_N \rightarrow \mathbb{P}_{\mathbf{x}|\theta_0}. \quad (9)$$

From the theorem statement we will assume (8) hold for almost every sequence $(\mathbf{x}_i)_{i \geq 1}$ sampled under θ_0 . From Varadaran’s theorem (see Dudley, 2018, Theorem 11.4.1) the same is true for (9). So it is almost sure that both hold. For the remainder of the proof we fix $(\mathbf{x}_i)_{i \geq 1}$ such that this is the case.

²Recall the notation $\mathbb{P}_{\mathbf{x}|\theta}$ was introduced at the start of Appendix A.

Part 1 We will show weak convergence of $\mathbb{P}_{\mathbf{x}|\mathbf{s}_N}^N$ to $\mathbb{P}_{\mathbf{x}|\theta_0}$.

Let θ_N be a random variable with distribution $\mathbb{P}_{\theta|\mathbf{s}_N}^N$. Select any continuous bounded $h : \mathbb{R}^{d_x} \rightarrow \mathbb{R}$. By assumption 3, (8) and the continuous mapping theorem, $\text{plim } h(G_{\theta_N}(\mathbf{u})) = h(G_{\theta_0}(\mathbf{u}))$. Since h is bounded we can apply dominated convergence to give

$$\mathbb{E}[h(G_{\theta_N}(\mathbf{u}))] \rightarrow \mathbb{E}[h(G_{\theta_0}(\mathbf{u}))].$$

Thus we get the required result

$$\mathbb{E}_{\mathbb{P}_{\mathbf{x}|\mathbf{s}_N}^N} [h(\mathbf{x})] \rightarrow \mathbb{E}_{\mathbb{P}_{\mathbf{x}|\theta_0}} [h(\mathbf{x})].$$

Part 2 We will show $\text{MMD}(\mathbb{P}_{\mathbf{x}|\mathbf{s}_N}^N, \hat{\mathbb{P}}_N) \rightarrow 0$.

By the triangle inequality

$$\text{MMD}(\mathbb{P}_{\mathbf{x}|\mathbf{s}_N}^N, \hat{\mathbb{P}}_N) \leq \text{MMD}(\mathbb{P}_{\mathbf{x}|\mathbf{s}_N}^N, \mathbb{P}_{\mathbf{x}|\theta_0}) + \text{MMD}(\mathbb{P}_{\mathbf{x}|\theta_0}, \hat{\mathbb{P}}_N).$$

Both terms converge to zero. For the first this follows from Part 1 and Remark A.1. For the second term this follows from (9) and Remark A.1.

Part 3 We will show $\text{MMD}(\mathbb{P}_{\mathbf{x}|\mathbf{s}_N^*}^N, \mathbb{P}_{\mathbf{x}|\theta_0}) \rightarrow 0$.

By the triangle inequality

$$\text{MMD}(\mathbb{P}_{\mathbf{x}|\mathbf{s}_N^*}^N, \mathbb{P}_{\mathbf{x}|\theta_0}) \leq \text{MMD}(\mathbb{P}_{\mathbf{x}|\mathbf{s}_N^*}^N, \hat{\mathbb{P}}_N) + \text{MMD}(\mathbb{P}_{\mathbf{x}|\theta_0}, \hat{\mathbb{P}}_N)$$

Again, the second term converges to zero by (9) and Remark A.1. To show the first term converges to zero, define

$$A_N = \text{MMD}(\mathbb{P}_{\mathbf{x}|\mathbf{s}_N^*}^N, \hat{\mathbb{P}}_N), \quad B_N = \text{MMD}(\mathbb{P}_{\mathbf{x}|\theta_0}^N, \hat{\mathbb{P}}_N).$$

Then $A_N \geq 0$, and $A_N \leq B_N$ from the definition of \mathbf{s}_N^* . Since $B_N \rightarrow 0$ by Part 2, we have $A_N \rightarrow 0$.

Part 4 Finally, $\mathbb{P}_{\theta|\mathbf{s}_N^*}^N$ weakly converges to δ_{θ_0} by Part 3, assumption 4 and Remark A.1.

B. Choice of divergence

As discussed in Section 3.1, the choice of divergence for the minimum-distance summaries objective, Equation (1) is crucial, as our main goal is to obtain a *robust* MDS. In order to do so, we have opted to use the MMD, which has strong robustness properties that is inherited with the MDS. Alternatively, when using the decoder model which estimates the summary-conditional data distribution with a flow-based model, such models allow for exact density evaluation, and we are able to use the forward KL divergence, which corresponds to maximum-likelihood.

We provide empirical results comparing the KL-divergence based MDS with the MMD MDS 3.2 in Figure 6, under the same Gaussian setup as Appendix D.1. As we can see, this experiment verifies that the MMD is indeed robust, and that the KL is not a robust objective, as it performs similarly to the baseline NPE under contamination.

C. Detecting model misspecification

The MMD was initially motivated as a two-sample test (Gretton et al., 2012) and has been exploited to detect model misspecification in previous SBI work (Schmitt et al., 2024). We propose a simple procedure to detect model misspecification using our trained decoder mean embedding $\hat{\mu}_\omega(\mathbf{s})$. We do this by calibrating a null distribution with a α false positive rate, on held-out validation data pairs $(\mathbf{x}_{1:N}, \mathbf{s})$, specifically by calculating the test statistics $\hat{\text{MMD}} = \|\hat{\mu}_\omega(\mathbf{s}) - \frac{1}{N} \sum_{n=1}^N \mathbf{z}(\mathbf{x}_n)\|_2^2$, and taking the $1 - \alpha$ quantile of this test statistics distribution, τ . Then, we only proceed with the adaptation for an observed dataset $\tilde{\mathbf{x}}$ if $\|\hat{\mu}_\omega(\mathbf{s}_0) - \hat{\mu}_{\text{obs}}\|_2^2 > \tau$, where $\mathbf{s}_0 = f(\tilde{\mathbf{x}})$.

We provide empirical results showing the empirical Type-I error and power of the model misspecification procedure in Figures 7 and 8 using the Gaussian setup in Appendix D.1. In particular, note that the left plot of Figure 8 confirms the sudden drop result discussed in Section 6.1, as this is due to the false negative from the contamination not being severe enough to trigger adaptation.

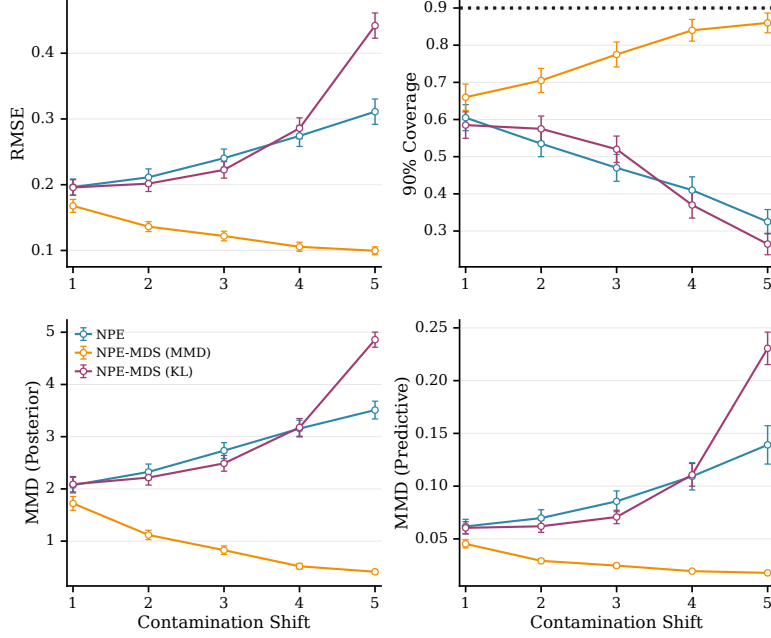


Figure 6. Comparison between KL-based MDS and MMD-based MDS, for increasing contamination shift.

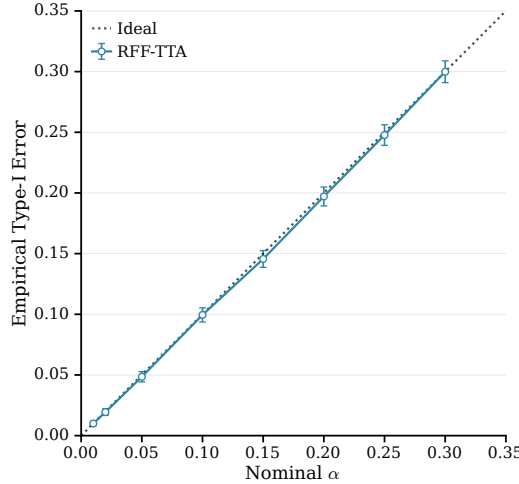


Figure 7. Empirical false positive rate for misspecification detection using the Gaussian task in Appendix D.1

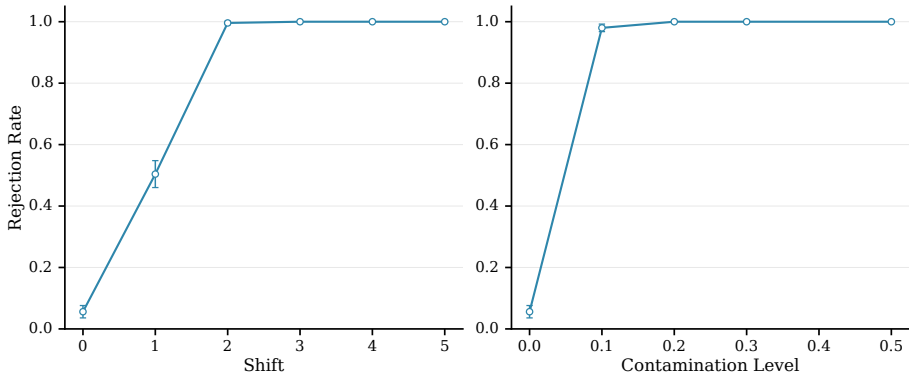


Figure 8. Rejection rate for misspecification detection using the Gaussian task in Appendix D.1, with increasing outlier shift and contamination proportion

D. Further experimental details and results

In this section, we provide further details and additional results, based on the experiments discussed in Section 6.

In all our experiments, we require the training of conditional density estimator for neural posterior estimators and the decoder model proposed in our MDS approach. We use the `sbi` package (Boelts et al., 2025) for the training of the required conditional density estimators. For both the NPE and decoder model, a neural spline flow (Durkan et al.) was used as the density estimator, with default configurations from `sbi`. The Adam (Kingma & Ba) optimizer was used with a learning rate of 5×10^{-4} and the density estimators were trained until convergence.

For the MDS algorithm with random Fourier features, the feature approximations corresponding to the RBF kernel were obtained with the `scikit-learn` package (Pedregosa et al.), using the standard median heuristic for the tuning of the bandwidth hyperparameter, and a fixed dimension of 512 for the dimension of the feature space. This feature approximation is used to obtain empirical mean embeddings of training data, which we subsequently use to train a standard fully-connected neural network with 2 hidden layers with 256 units per layer, giving us an amortized conditional mean embedding estimate with respect to \mathbf{s} . During test-time, we use the L-BFGS optimization algorithm (Liu & Nocedal, 1989) with line search as implemented in the `PyTorch` package (Paszke et al.) to obtain the adapted MDS in Equation 2. For the decoder model variant of the MDS algorithm, after training of the amortized decoder model with training data, we use the Adam optimizer (Kingma & Ba) to directly solve an empirical estimate of Equation 1 by drawing samples from the decoder model. As discussed in Appendix C, we reserve 5% of the training data for calibration, which is not used in the pretraining of the conditional mean embedding or decoder model.

For the Noisy NPE of Ward et al. (2022), the spike-and-slab error model was used. Following the notation of \mathbf{y} as the summary statistic and \mathbf{x} as the unobserved latent variable, the error model is (see Equation 8 of Ward et al. (2022)):

$$p(\mathbf{y} \mid \mathbf{x}) = \prod_{j=1}^D [(1 - \rho)N(x_j, \sigma^2) + \rho \text{Cau}(x_j, \tau)]$$

We set $\rho = 0.5$, $\sigma = 0.01$ and $\tau = 0.2$. As we use the NNPE variant of the algorithm, we directly incorporate this to the simulator model, and train an amortized NPE directly. The NPE-RS method of Huang et al. (2023) was trained by augmenting the standard NPE negative log-likelihood loss function with a regularization term, $\lambda \cdot \text{MMD}^2[f_\phi(\mathbf{x}_{1:N}), f_\phi(\tilde{\mathbf{x}}_{1:N})]$, where $\mathbf{x}_{1:N}$, $\tilde{\mathbf{x}}_{1:N}$ are training and observed samples respectively. In particular, this requires use of a neural summary statistic f_ϕ in order to minimize the regularization term. We use grid search of $\lambda \in \{0.1, 1.0, 5.0, 10.0\}$, and provide the results for the best performing model for each metric. For the OC-SVM (Schölkopf et al.) approach, we fit a one-class SVM using `scikit-learn` (Pedregosa et al.) on training data using the Gaussian kernel with median heuristic, calibrate a threshold using a false positive rate of 5%, mimicking the approach of the MDS, and remove outliers based on the OC-SVM. We then resample from the remaining inliers to maintain the same fixed observations.

In all our tasks, we use datasets $\mathbf{x}_{1:N}$ which $N = 100$, and 100 different test datasets, each corresponding to a true parameter θ^* . The randomness of the error bars in all plots are with respect to the 100 test datasets. For parameter estimation accuracy, we calculate the RMSE over the parameter dimensions, $\sqrt{\frac{1}{d_\theta} \|\bar{\theta} - \theta^*\|_2^2}$, where $\bar{\theta}$ is the posterior mean from the posterior samples for each method. For the calibration of the posterior, we calculate the coverage, by estimating the credible intervals $L_j = Q_{\alpha/2}(\{\theta_j^{(s)}\}_{s=1}^M)$, $U_j = Q_{1-\alpha/2}(\{\theta_j^{(s)}\}_{s=1}^M)$ using posterior samples, and obtain coverage $\mathbf{1}[L_j \leq \theta_j^* \leq U_j]$, which is then averaged over the parameter dimensions. We also obtain posterior predictive metric by comparing the posterior predictive distribution, estimated by resampling from the obtained posterior samples with the simulator model, against the clean, uncontaminated test dataset. Since the MDS approach operates entirely on the summary-space and original data-space, it is natural to compare against the oracle summary, which is the summary statistic of the clean, uncontaminated test dataset, which we do by comparing the Euclidean distance against the obtained MDS. Finally, where possible, such as with the Gaussian task, we compare with the reference posterior directly using the MMD.

D.1. Gaussian task

In this section, we discuss the experimental setup for Section 6.1, as well as additional results and experiments based on this setup.

The Gaussian task is based on the following model:

Prior	$\theta \sim \mathcal{N}_d(\mathbf{0}, I_d)$
Simulator	$\mathbf{x}_{1:N} = (\mathbf{x}_1, \dots, \mathbf{x}_N), \mathbf{x}_i \mid \theta \sim \mathcal{N}_d(\theta, I_d), i = 1, \dots, N$
Summary statistic	$f_\phi : \mathbb{R}^{N \times d} \rightarrow \mathbb{R}^d$
Dimensionality	$\theta \in \mathbb{R}^d, \mathbf{x}_i \in \mathbb{R}^d, \mathbf{x}_{1:N} \in \mathbb{R}^{N \times d}$

This provides a closed-form conjugate posterior distribution, which we use to provide an exact measure of the accuracy of our posterior approximation. Note that, for this task, we use a trained neural summary statistic f_ϕ (parameterized as a fully-connected neural network), which is learnt jointly with the NPE, which allows us to use the NPE-RS approach. We use 50000 training datasets, and 100 test datasets for evaluation. We use $d = 2, N = 100$ unless stated otherwise.

Misspecification For a test dataset $\mathbf{x}_{1:N}$ generated from true parameter θ^* , each observation is independently replaced by a shifted outlier with probability ϵ : $\tilde{\mathbf{x}}_i = \mathbf{x}_i$ w.p. $1 - \epsilon$, and $\tilde{\mathbf{x}}_i = z_i \cdot \delta$ w.p. ϵ , where $z_i \sim \text{Unif}\{-1, +1\}$. where $\delta > 0$ controls the outlier magnitude. We vary $\epsilon \in \{0.1, 0.2, 0.3, 0.5\}$ with fixed magnitude $\delta = 3$, and vary $\delta \in \{1, 2, 3, 4, 5\}$ with fixed $\epsilon = 0.2$. This misspecification is based on Experiment 2 of Elsemüller et al. (2025).

In addition to the plot provided in Figure 2, we provide additional plots below. Furthermore, we show the resulting MDS posterior adaptation from four different test datasets in Figure 13.

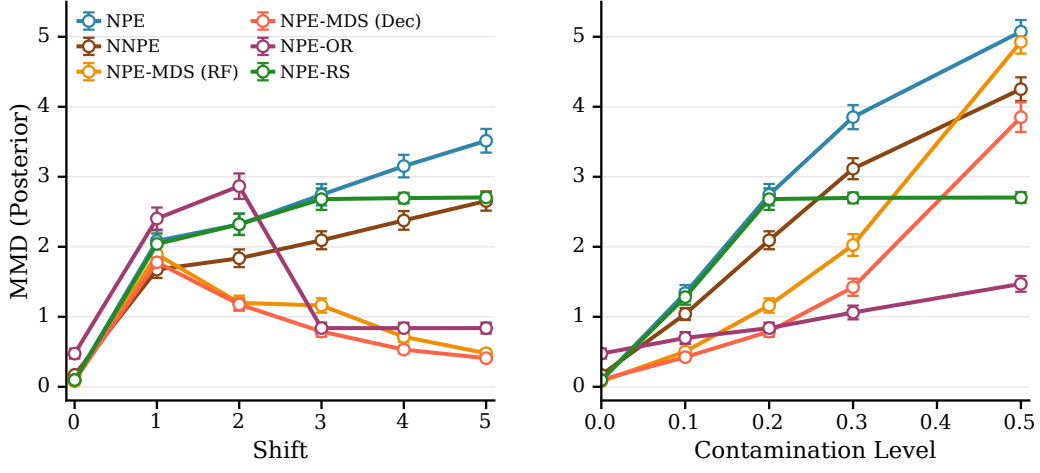


Figure 9. MMD between estimated posterior and reference true posterior for Gaussian task (Appendix D.1)

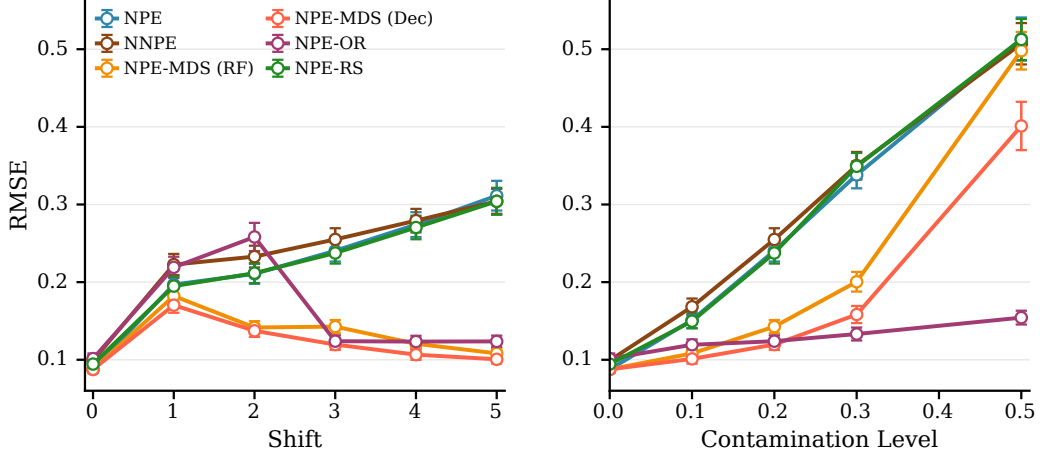


Figure 10. RMSE between estimated posterior means and true parameter for Gaussian task (Appendix D.1)

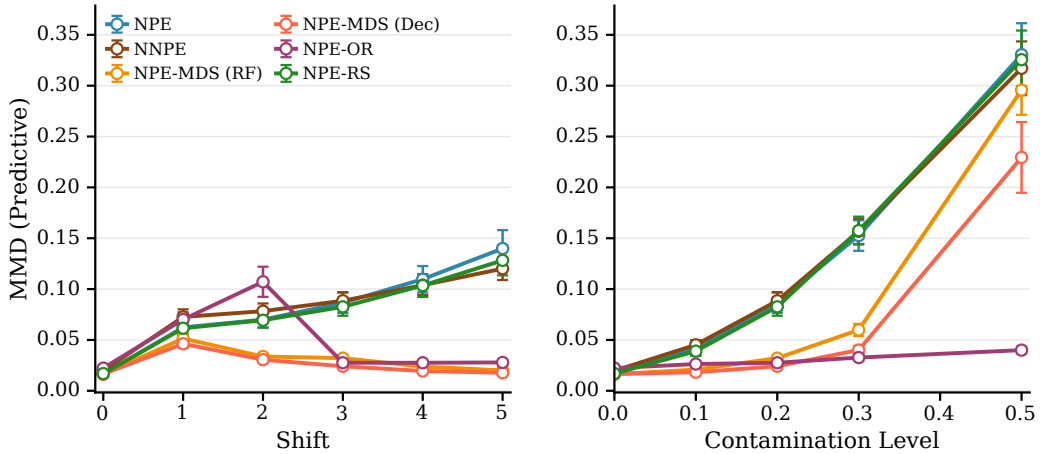


Figure 11. MMD between estimated posterior predictive and uncontaminated test dataset for Gaussian task (Appendix D.1)

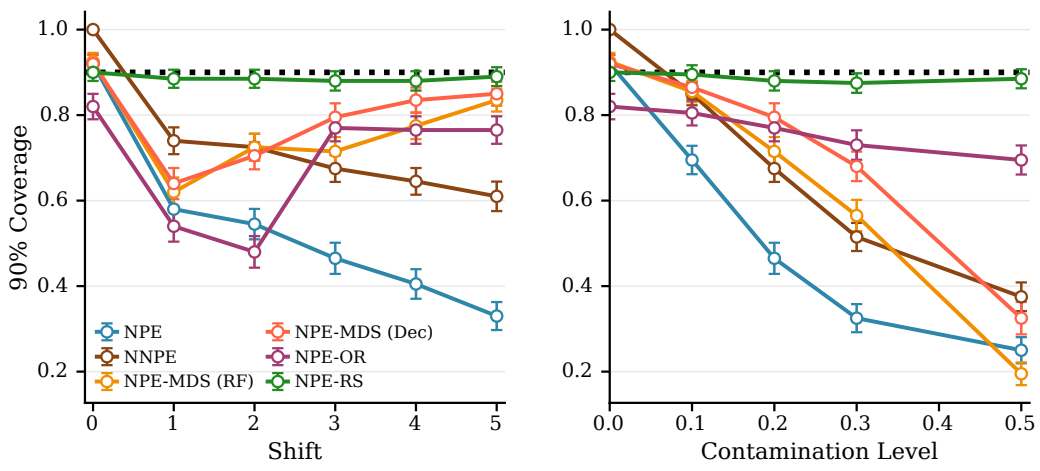


Figure 12. Coverage of estimated posterior for Gaussian task (Appendix D.1)

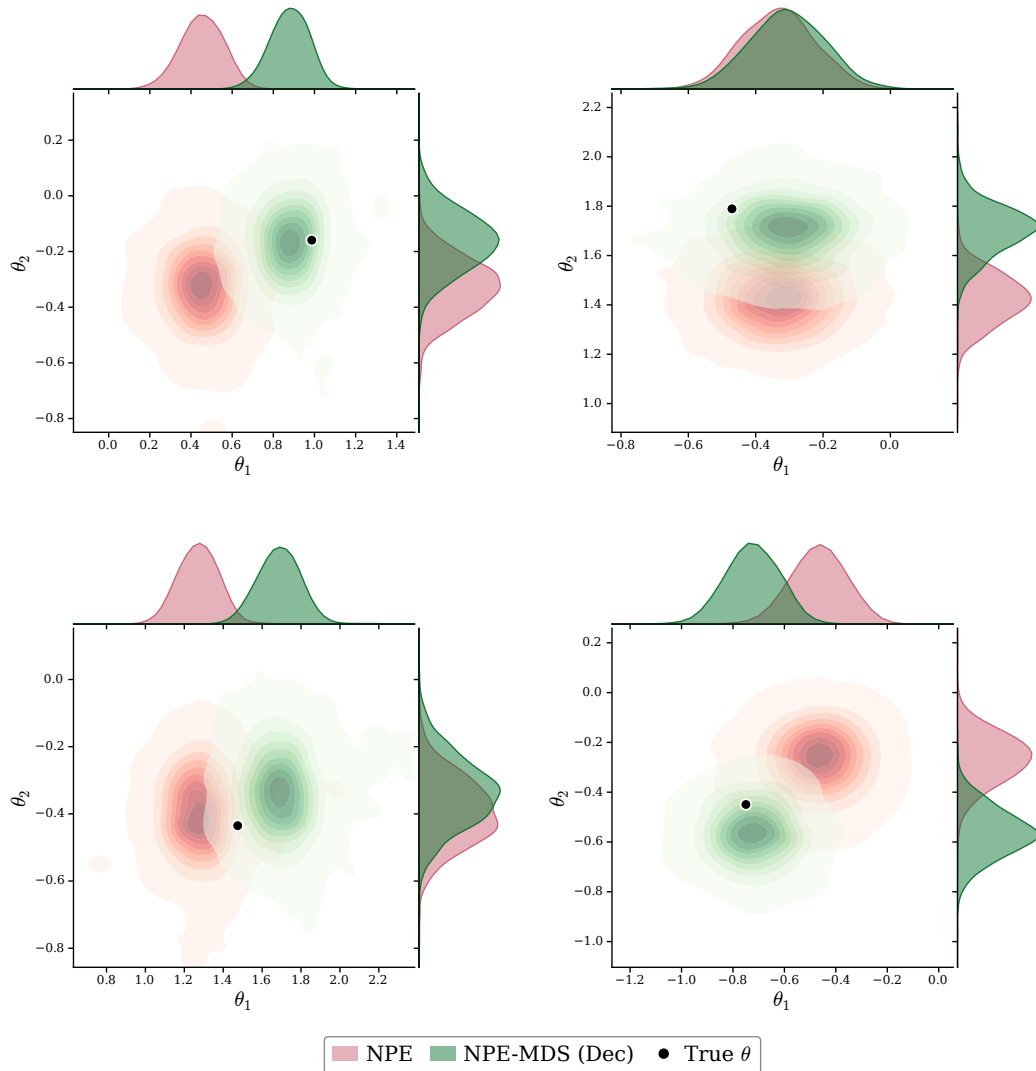


Figure 13. Posterior distributions before and after MDS adaptation for Gaussian task, for four test datasets (Appendix D.1)

D.1.1. ABLATION STUDIES

In this section, we provide ablation studies to test the sensitivity of our proposed MDS approach against increasing number of observations N and observation dimension d_x .

Sample size ablation We use broadly the same setup as before, but changing the number of observations $N \in \{5, 10, 50, 100, 200, 500\}$. For the misspecification, we use $\delta = 5, \epsilon = 0.2$. We furthermore use directly the sample mean as the summary statistic. The results are provided in Figure 14. We find that overall, NPE-MDS obtains better robustness compared to both NPE and NNPE, although the improvement increases as N increases.

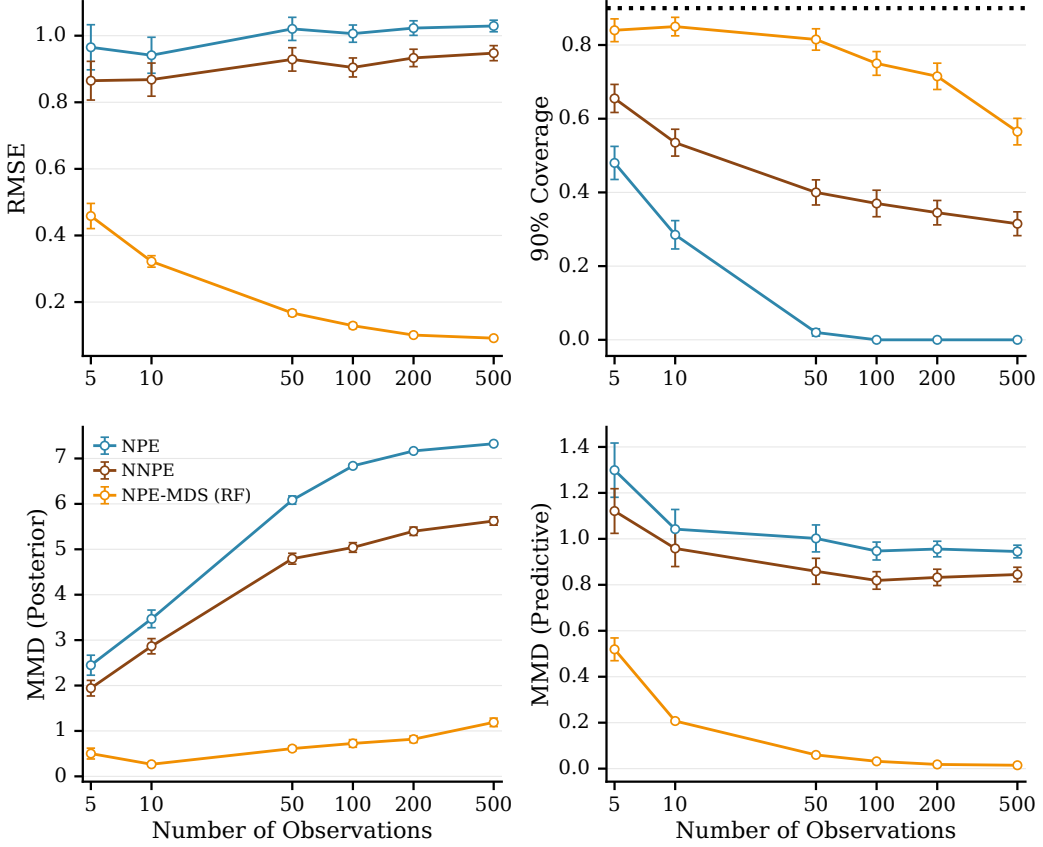


Figure 14. Results for ablation with increasing number of observations (Appendix D.1.1)

Data dimension ablation As we would like to investigate the sensitivity of our method to increasing observation dimension, increasing the dimensions of the Gaussian task directly would not be suitable as that would lead to an increase in the parameter and importantly, the summary statistic dimension. In order to keep both these variables fixed, we propose a slight alteration to the Gaussian task, using a Gaussian factor model $\mathbf{x}_i \mid \theta \sim N(A\theta, I)$, where $A \in \mathbb{R}^{D \times 2}$ is a random projection matrix. Which we then use as a summary statistic $A^+ \cdot \bar{\mathbf{x}}_{1:N}$. This allows us to change the dimensionality of the observations $D \in \{2, 5, 10, 50, 100\}$ while keeping both the parameter and summary statistic dimension fixed at the original setting of 2. For the misspecification, we use $\delta = 5, \epsilon = 0.3$. The results for this ablation study is provided in Figure 15. We find that, while the NPE-MDS overall still provides improvement on the robustness compared to both the NPE and NNPE, this gap decreases as the observation dimension increases.

D.1.2. NPE-PFN

NPE-PFN (Vetter et al., 2025) provides an alternate approximation to the Bayesian posterior distribution based on probabilistic foundation models, performing Bayesian inference through in-context learning. In this setting, as we would like to ideally avoid modifying the pretrained NPE-PFN directly, the test-time paradigm is a natural fit, for which the MDS

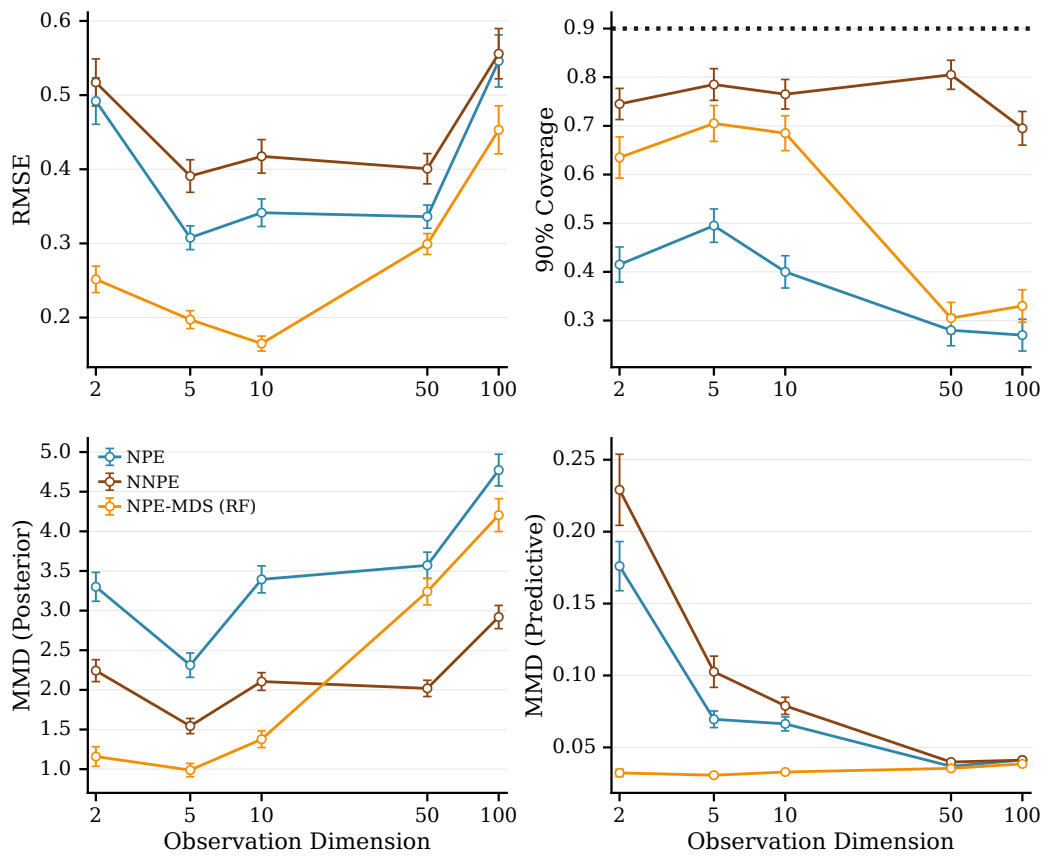


Figure 15. Results for ablation with increasing number of dimensions (Appendix D.1.1)

simply adapts the query summary for robustness. We use the same Gaussian task setup as before. The results are provided in Figures 16, 17, 18 and 19, and we find that the MDS can provide robustness benefits in this setting.

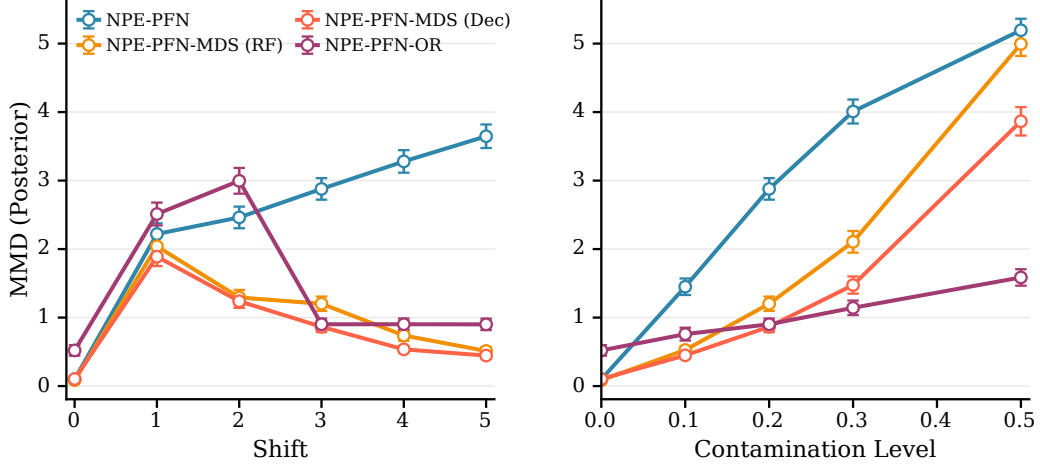


Figure 16. MMD between estimated posterior (NPE-PFN) and reference true posterior for Gaussian task (Appendix D.1.2)

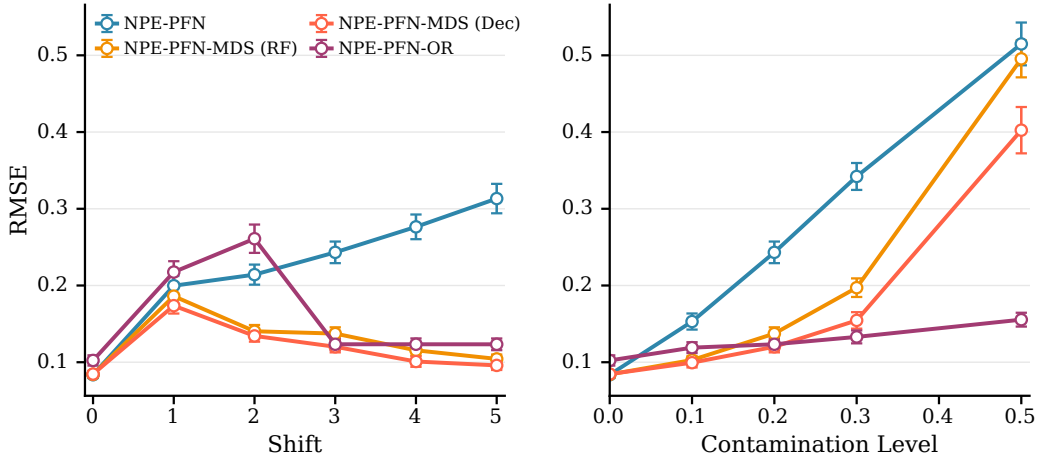


Figure 17. RMSE between estimated posterior means (NPE-PFN) and true parameter for Gaussian task (Appendix D.1.2)

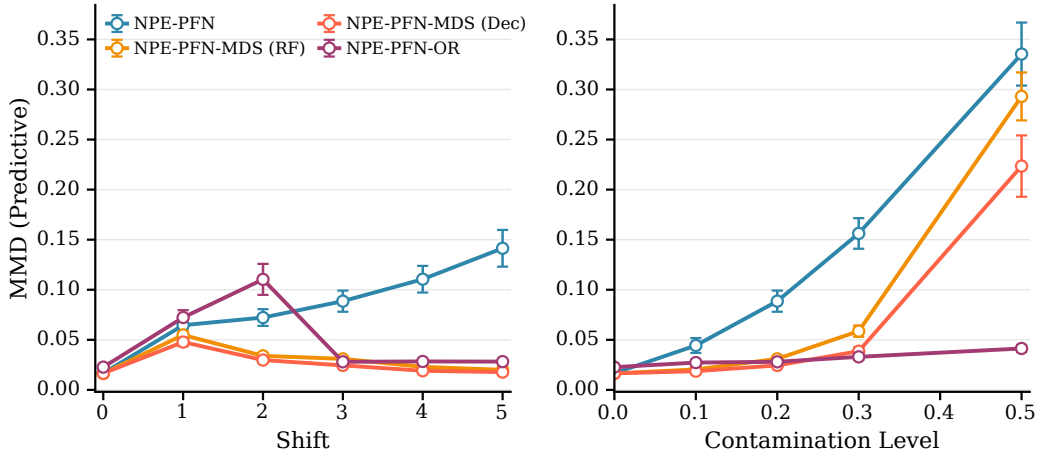


Figure 18. MMD between estimated posterior predictive (NPE-PFN) and uncontaminated test dataset for Gaussian task (Appendix D.1.2)

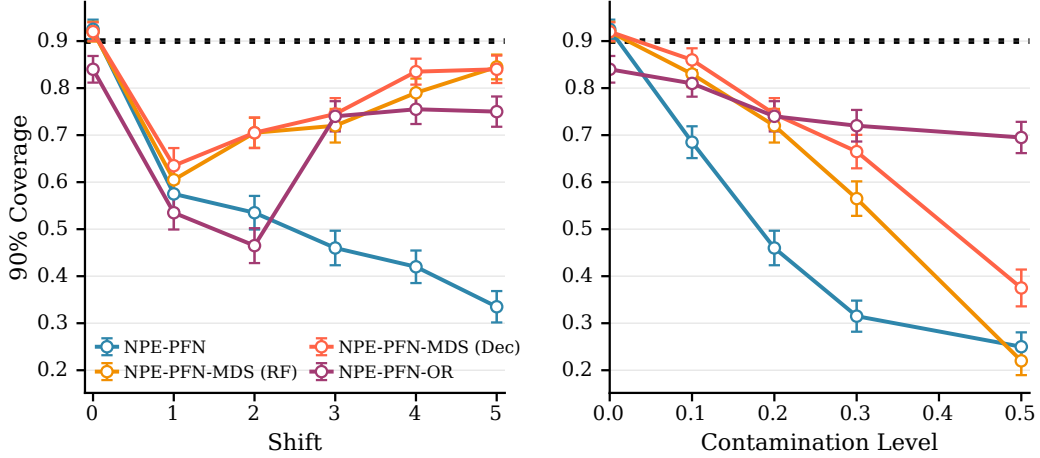


Figure 19. Coverage of estimated posterior (NPE-PFN) (Appendix D.1.2)

D.2. OUP task

The Ornstein–Uhlenbeck process (OUP) is defined by a mean-reverting stochastic differential equation, and is based on the experiment provided in [Huang et al. \(2023\)](#). One key distinction is that we use a fixed summary statistic, instead of a learnt neural summary statistic that was done in their setup. The summary statistic (s_1, s_2, s_3) is the mean, variance, and lag-1 autocorrelation respectively, which is averaged over the trajectories and datasets. We use $T = 25$ and $N = 100$ trajectories per dataset. The diffusion variance is set at $\sigma^2 = 0.1$, and initial conditions was set starting from $X_0 = 10$, and the SDE was discretized with a standard Euler-Maruyama scheme. We use 10000 training datasets for the NPE training.

Contamination was induced by replacing a fraction ϵ of trajectories with contaminated trajectories, generated from a contaminated parameter of $\theta = (-0.5, 1.0)$ and with $\sigma^2 = 0.5$.

Prior $(\theta_1, \theta_2) \sim U[0, 2] \times U[-2, 2]$

Simulator $dX_t = \theta_1[\exp(\theta_2) - X_t]dt + \sigma dW_t,$

Summary statistic $s(\mathbf{x}_{1:N}) = (s_1, s_2, s_3)$, where $\mathbf{x}_{1:N} = \mathbf{X} \in \mathbb{R}^{N \times T}$:

$$s_1 = \frac{1}{NT} \sum_{n=1}^N \sum_{t=1}^T \mathbf{X}_{n,t}$$

$$s_2 = \frac{1}{NT} \sum_{n=1}^N \sum_{t=1}^T (\mathbf{X}_{n,t} - s_1)^2$$

$$s_3 = \text{corr}\left(\text{vec}(\mathbf{X}_{:,1:T-1}), \text{vec}(\mathbf{X}_{:,2:T})\right).$$

Dimensionality $\theta \in \mathbb{R}^2$, $\mathbf{x}_i \in \mathbb{R}^T$, $\mathbf{x}_{1:N} \in \mathbb{R}^{N \times T}$

We provide the results and posteriors for the OUP task in Figures 20 and 21.

D.3. SIR task

The SIR (Susceptible-Infected-Recovered) model is a classic epidemiological model which models the spread of infectious disease through a population. This setup is similar to [Ward et al. \(2022\)](#). This particular SIR variant is a stochastic variant, which has standard ODE dynamics for S, I, R and a mean-reverting diffusion process for the reproduction number R_0 , which is coupled to the ODE through the effective transmission rate $\beta_{\text{eff}} = \gamma \cdot R_0$. In the diffusion process, for R_0 , we have $\bar{R}_0 = \beta/\gamma$ and set $\sigma = \eta = 0.05$. The system is initialized with $(S_0, I_0, R_0) = (0.999, 0.001, 0)$, and integrated with a standard Euler-Maruyama scheme over $T = 365$ days, giving daily infection counts $X_t = N \cdot I_t$ where the population $N = 10000$. We simulate 100 trajectories for each parameter, and the parameters to be inferred are the infection and recovery rate, β, γ respectively. We use 10000 training datasets for the NPE training.

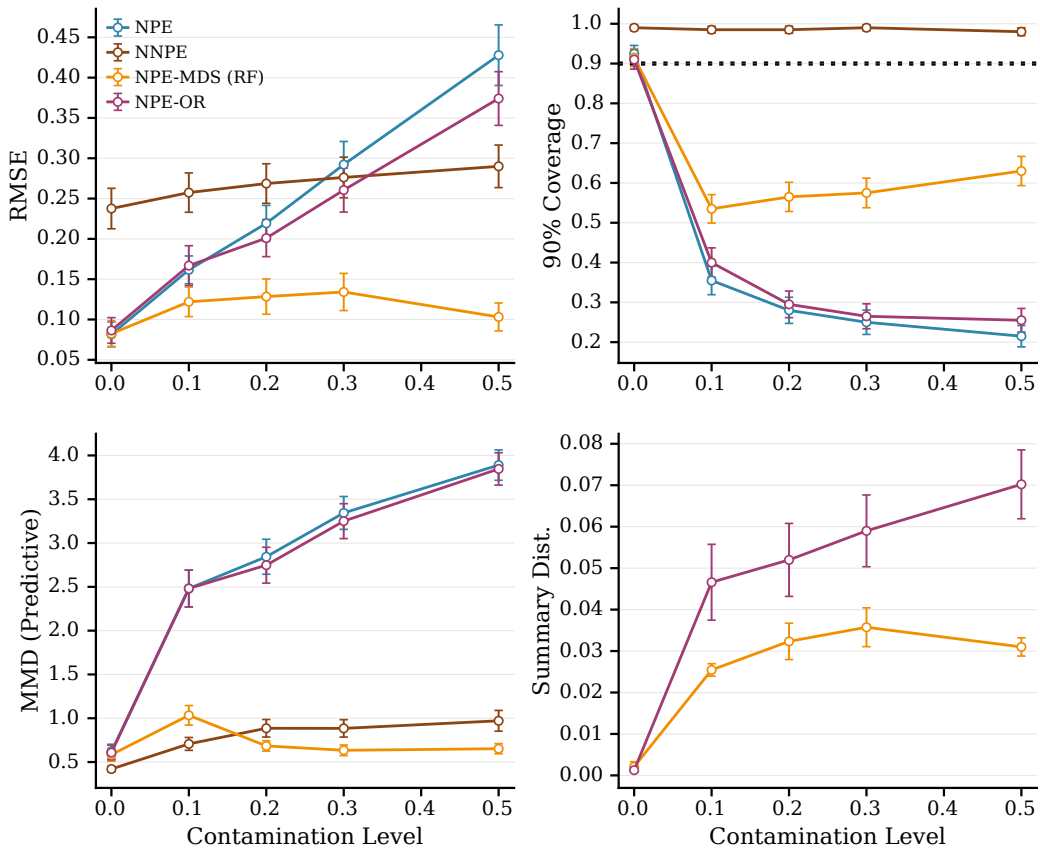


Figure 20. Results for OUP task (Appendix D.2)

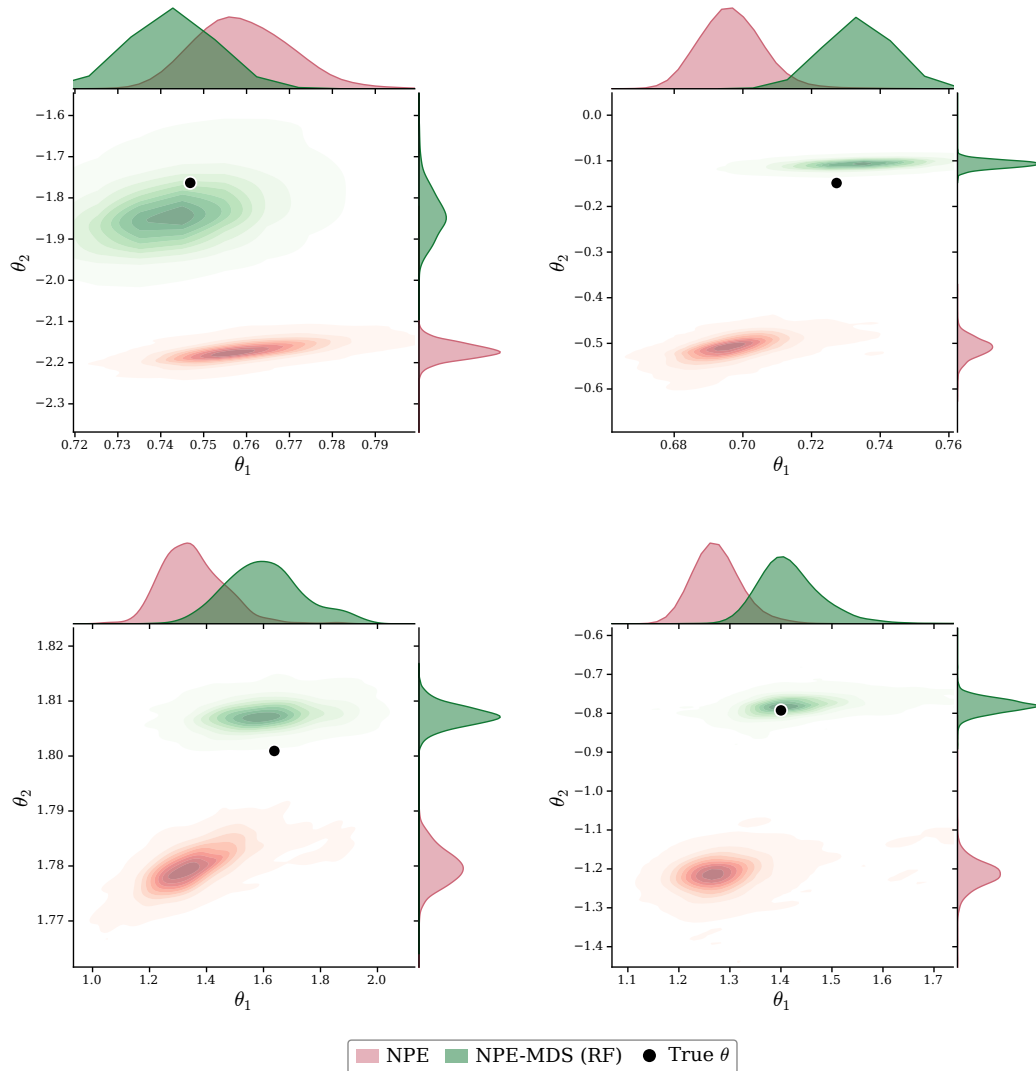


Figure 21. Posterior distributions before and after MDS adaptation for OUP task for four test dataset (Appendix D.2)

Following Ward et al. (2022), for the summary statistic (S_1, \dots, S_6) , we take this to be the log mean infections, log median infections, log peak infections, log day of peak, log day when 50% of cumulative infections are reached, and the lag-1 autocorrelation, which is averaged across trajectories.

Model misspecification is introduced through weekend underreporting, for a fraction ϵ of the trajectories, weekend infection counts are undereported (by 5%), and redistributed to the following Monday.

Prior $(\beta, \gamma) \sim U[\{(\beta, \gamma) : 0 < \gamma < \beta < 0.5\}]$.

$$\frac{dS}{dt} = -\beta_{\text{eff}}(t)SI,$$

$$\frac{dI}{dt} = \beta_{\text{eff}}(t)SI - \gamma I,$$

$$\frac{dR}{dt} = \gamma I,$$

$$dR_0 = \eta(\bar{R}_0 - R_0)dt + \sigma\sqrt{|R_0|}dW_t$$

Summary statistic $\mathbf{S}(\mathbf{x}_{1:N}) = (S_1, \dots, S_6)$, where $\mathbf{x}_{1:N} = \mathbf{X} \in \mathbb{R}^{N \times T}$

Dimensionality $\theta \in \mathbb{R}^2$, $\mathbf{x}_i \in \mathbb{R}^T$, $\mathbf{x}_{1:N} \in \mathbb{R}^{N \times T}$, $\mathbf{S} \in \mathbb{R}^6$.

We provide results and posteriors for the SIR task in Figures 22 and 23.

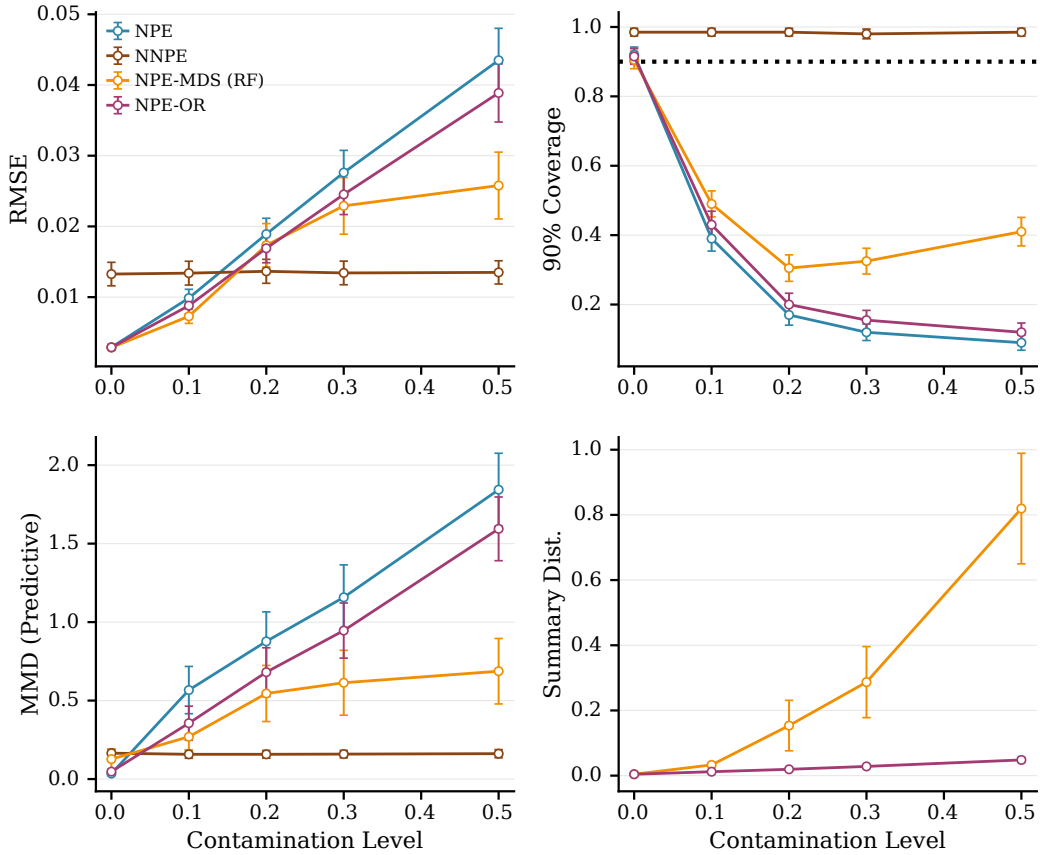


Figure 22. Results for SIR task (Appendix D.3)

D.4. Cryo-EM task

Cryo-electron microscopy (cryo-EM) is an imaging technique that captures projected 2D images of 3D biomolecules, whose configuration (conformational state) varies across images. In particular, this problem setting is especially challenging due to the presence of nuisance variables, such as the orientation of the image and measurement noise. We refer the interested

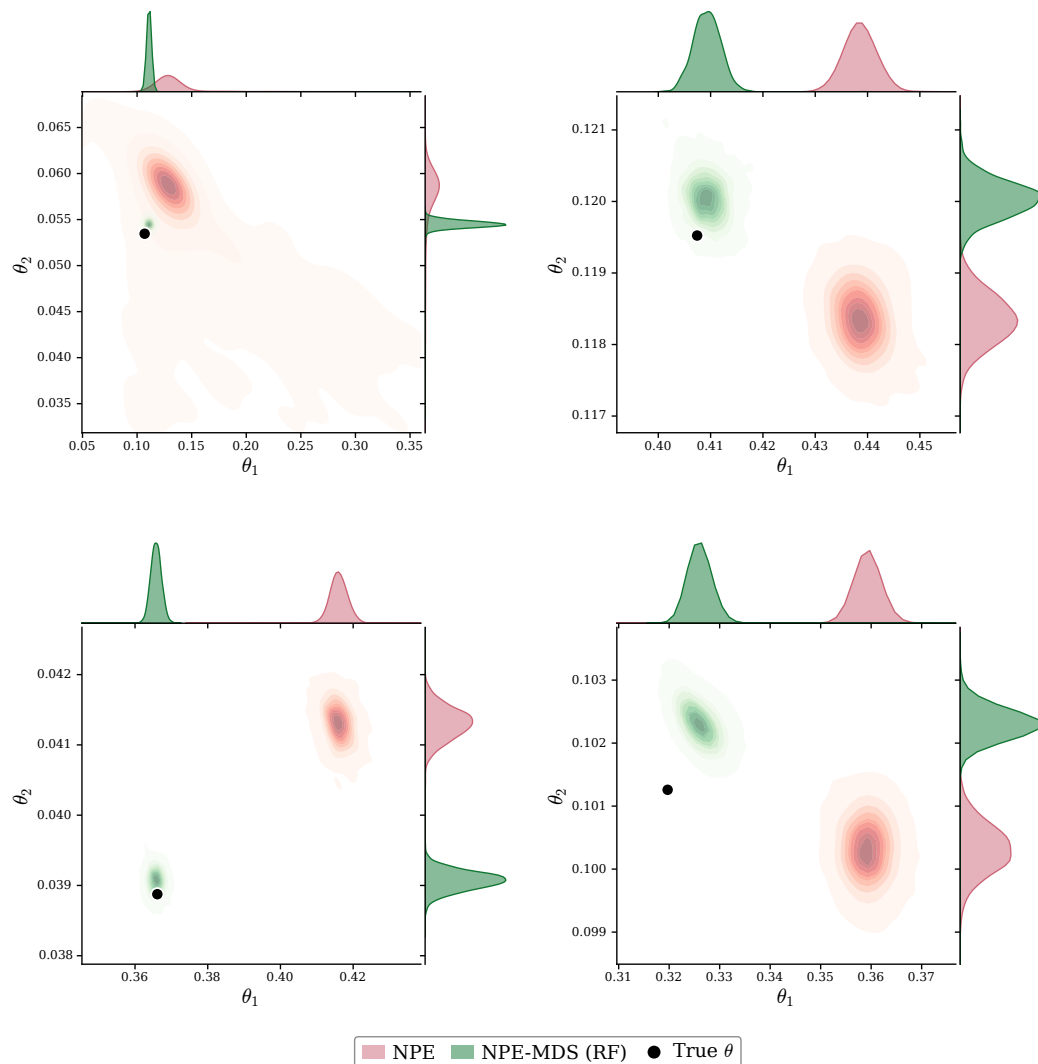


Figure 23. Posterior distributions before and after MDS adaptation for SIR task for four test dataset (Appendix D.3)

reader to Dingeldein et al. (2025); Evans et al. (2025) for further details about this problem setting. We use the HSP90 (Heatshock protein 90) model, provided as a benchmark in the `cryoSBI` package in (Dingeldein et al., 2025). For each conformational state θ , we simulate a 32×32 image, and the goal is to estimate a conformational index θ with prior as discrete uniform over $K = 20$ indices. As summary statistic, we compute the per-image skewness, kurtosis and intensity range, and aggregate this across the dataset of $N = 100$ images, and use the resulting mean and standard deviation, giving a 6 dimensional summary statistic. We use 15000 training datasets for the NPE training.

Model misspecification is induced by contaminating ϵ proportion of the images in the dataset with pure Gaussian noise, which simulates measurement or equipment error that is common in realistic cryo-EM settings.

We provide results and posteriors for the cryo-EM task in Figures 24 and 25.

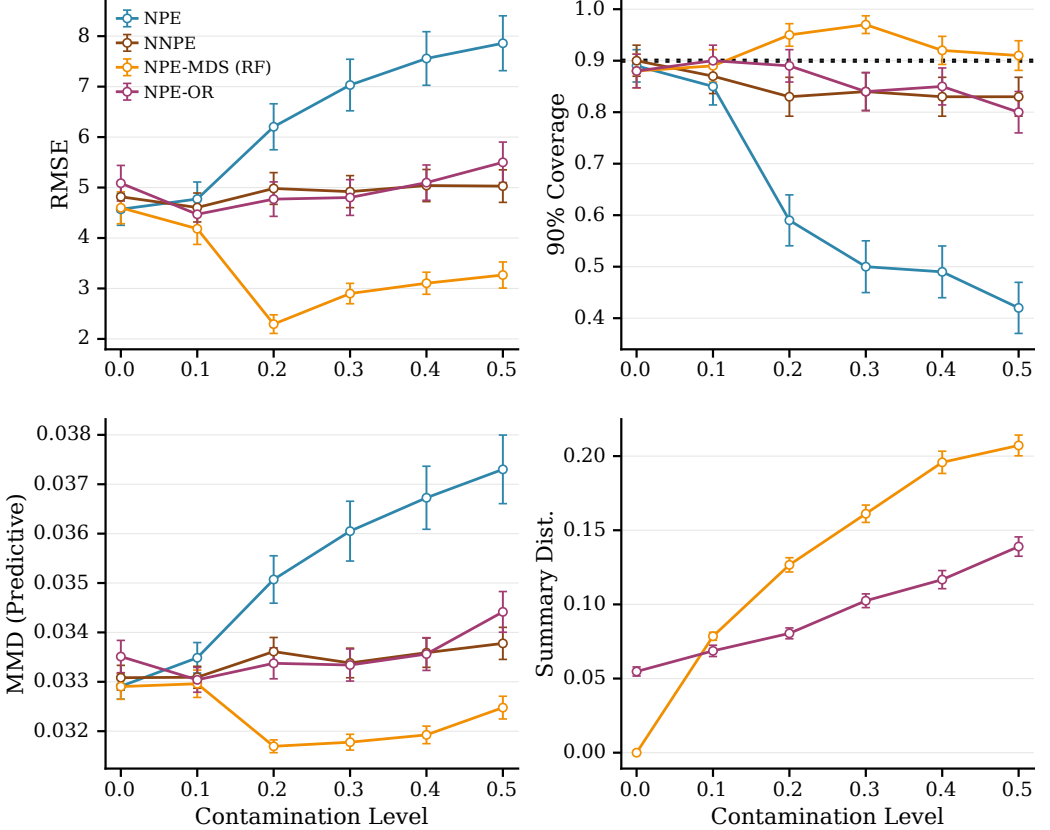


Figure 24. Results for cryo-EM task (Appendix D.4)

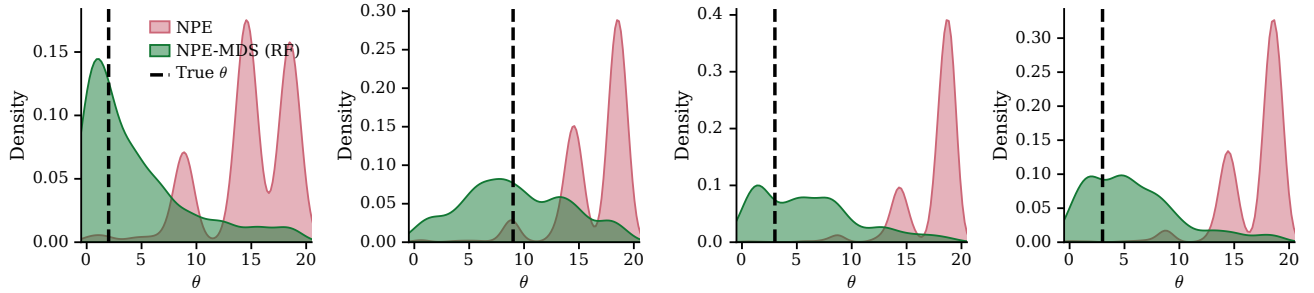


Figure 25. Posterior distributions before and after MDS adaptation for cryo-EM task for four test dataset (Appendix D.4)